scientific reports

Check for updates

OPEN

Exploring the active ingredients and potential mechanisms of Pingchan granules in Parkinson's disease treatment through network pharmacology and transcriptomics

Qiu-Han Xu[1,3], Yi-Ling Wang[1,3], Cheng Wang[2,3], Si-Si Jiang[1], Bao-Rong Zhang[1]✉ & Jun Tian[1]✉

Parkinson's disease (PD), the second most prevalent neurodegenerative disorder, poses significant challenges to single-target therapeutic strategies due to its complex etiology. This has driven interest in multi-target approaches, particularly those leveraging natural compounds. Pingchan granules (PCG), a traditional Chinese medicine composed of plant- and animal-derived compounds, have shown efficacy in alleviating PD symptoms. Here, we identify 96 PCG-associated anti-PD targets, enriched in neuronal synaptic signaling and G protein-coupled receptor pathways. Through protein-protein interaction network analysis of anti-PD targets and random forest modeling of substantia nigra transcriptomic data from PD patients, SLC6A3 and SRC emerged as central hub targets, with Mendelian randomization further validating SRC as a potential therapeutic target. Molecular docking and single-cell sequencing reveal that dauricine, PCG's principal active compound, binds strongly to SLC6A3 and SRC, modulating glucose metabolism pathways in dopaminergic neurons. These findings illuminate the molecular basis of PCG's therapeutic effects, offer a foundation for future drug development, and underscore the potential of dauricine as a targeted treatment for PD.

Keywords Parkinson's disease, Pingchan granules, Network Pharmacology, Single-cell nuclear sequencing, Molecular dynamics simulation, Mendelian randomization

Abbreviations

PD	Parkinson's Disease
PCG	Pingchan Granules
TCM	Traditional Chinese Medicine
GEO	Gene Expression Omnibus
RNA-seq	RNA Sequencing
snRNA-seq	Single-cell Nuclear RNA Sequencing
PPI	Protein-Protein Interaction
KEGG	Kyoto Encyclopedia of Genes and Genomes
GO	Gene Ontology
TF	Transcription Factor
miRNA	MicroRNA
GPCR	G Protein-Coupled Receptor
MAO	B-Monoamine Oxidase B
RMSD	Root Mean Square Deviation
AUC	Area Under the Curve
MR	Mendelian Randomization

[1]Department of Neurology, the Second Affiliated Hospital, School of Medicine, Zhejiang University, Hangzhou 310009, Zhejiang, China. [2]Department of Neurosurgey, the Second Affiliated Hospital, School of Medicine, Zhejiang University, Hangzhou, China. [3]Qiu-Han Xu, Yi-Ling Wang and Cheng Wang contributed equally to this work ✉email: brzhang@zju.edu.cn; juntian@zju.edu.cn

PD is a complex neurodegenerative movement disorder marked by the depletion of dopaminergic neurons in the midbrain's substantia nigra, resulting in a substantial reduction in dopamine levels in the striatum. The presence of Lewy bodies in the substantia nigra and locus coeruleus further characterizes its pathological features[1]. The etiology of PD is multifactorial, with contributing factors such as environmental exposure to pesticides, herbicides, and heavy metals, microbiota dysbiosis[2], and viral infections, including influenza and COVID-19, which have been linked to an elevated long-term risk of PD[3,4]. Predominantly identified by motor symptoms such as bradykinesia, static tremor, postural instability, and hypokinesia, PD progresses to encompass a noteworthy decline in functional abilities. This decline is evidenced by reduced muscle strength, compromised balance, and impaired gait performance[5]. Concurrently, a spectrum of non-motor symptoms emerges, including sleep disturbances, autonomic dysfunction, neuropsychiatric disorders, and cognitive impairment[6,7]. The amalgamation of these motor and non-motor symptoms poses a direct threat to the independent living of PD patients, resulting in substantial economic and global burdens[8,9].

The ultimate treatment goal for PD is to modify the disease's trajectory and impede the progression of associated symptoms. Current therapeutic strategies encompass both pharmaceutical and non-pharmacological approaches. From a pharmacological standpoint, primary interventions involve dopamine replacement therapy. Complementary non-pharmacological measures, such as exercise and physical therapy, form integral components of PD management. However, certain PD symptoms exhibit suboptimal responsiveness to dopaminergic drugs or deep brain stimulation (DBS), suggesting resistance to conventional treatments[5]. Consequently, an urgent imperative exists to deepen our understanding of the pathogenesis of PD and explore innovative medical interventions to address these treatment gaps.

PCG, a traditional Chinese medicine, exert substantial therapeutic efficacy across all stages of PD, displaying minimal side effects[10]. Serving as a complementary intervention to existing functional surgeries and anti-Parkinson drug treatments, PCG is formulated with six widely used traditional Chinese medicines (Lycium barbarum l., 12 g; Taxillus chinensis (DC.) Danser, 15 g; Gastrodia elata Blume, 9 g; Paeonia lactiflora Pall., 15 g; Arisaema erubescens (Wall.) Schott, 15 g; and Curcuma phaeocaulis Valeton, 9 g) and three common traditional Chinese medicines (Bombyx mori Linnaeus, 9 g; Buthus martensii Karsch, 3 g; and Scolopendra subspinipes mutilans l. Koch, 3 g). In numerous prior double-blind randomized controlled clinical trials, PCG has demonstrated effectiveness in addressing motor symptoms, including axial symptoms, bradykinesia, tremor, rigidity, and frozen gait, as well as motor complications such as dyskinesia and regression[10–12]. Notably, PCG extends its positive impact to non-motor symptoms, encompassing depression, anxiety, cognitive decline, and autonomic dysfunction[12]. Moreover, individuals taking PCG have reported a significant enhancement in their quality of daily life, accompanied by marked improvements in mobility functions, walking ability, and dynamic balance[11]. This collective evidence underscores the comprehensive benefits of PCG in the management of PD.

Research in Traditional Chinese Medicine (TCM) often involves complex compounds that interact with multiple pathological targets and pathways. Traditional pharmacological methods face limitations in comprehensively studying the mechanisms of TCM due to its multifaceted nature. Network pharmacology has emerged as a novel field within systems drug research, aiming to unravel the effects of drugs and their interactions with multiple targets[13]. This approach places emphasis on the synergy of multi-components, multi-channels, and multi-targets, making it particularly well-suited for the nuanced analysis of traditional Chinese medicine. Network pharmacology employs cutting-edge techniques such as virtual computing, high-throughput data analysis, and network database retrieval. It encompasses the construction of machine learning models, bioinformatics network development, and analysis of network topology. Through the integration of bioinformatics, computational prediction-based network pharmacology has evolved into a potent method for systematically uncovering the molecular-level biological mechanisms underpinning complex diseases and drug effects[14]. This method is increasingly applied to various domains of TCM treatment, spanning cardiovascular diseases, neurodegenerative diseases, cancer, and more. The versatility and depth of network pharmacology offer a powerful avenue for advancing our understanding of the intricate interactions between traditional Chinese medicine compounds and their biological targets.

This study employs a combination of network pharmacology and machine learning models to meticulously screen hub targets. Molecular docking technology and molecular dynamics simulation are utilized to predict the primary bioactive compounds, potential targets, and signaling pathways associated with the therapeutic effects of PCG in PD. The results of our investigation furnish a solid foundation for further research on the mechanism of action of PCG in the treatment of PD. The study's workflow is illustrated in Fig. 1.

Methods

Screening of active ingredients in PCG

In the Integrative Pharmacology-based Research Platform of Traditional Chinese Medicine (TCMIP, http://www.tcmip.cn/TCMIP/index.php/)[15], the search term included wolfberry, locust, peony, araceae, and Curcuma zedoary to retrieve related components and targets. Filtering conditions were set to OB ≥ 30% and DL ≥ 0.18. From the HERB database (http://herb.ac.cn/)[16], components related to Bombyx mori, Whole Scorpion, Centipede, and Gastrodia were obtained. Subsequently, the NCBI Pubchem database (https://pubchem.ncbi.nlm.nih.gov/)[17] was utilized to acquire the structural information of Bombyx Silkworm, Whole Scorpion, Centipede, and Gastrodia. The structural information, represented in heterogeneous SMILE formulas, was then input into the Swiss Target Prediction database (Swiss Target Prediction http://www.swisstargetprediction.ch)[18] to extract their targets. Finally, the UniProt database (https://www.uniprot.org/)[18] was employed to standardize these targets into gene names.

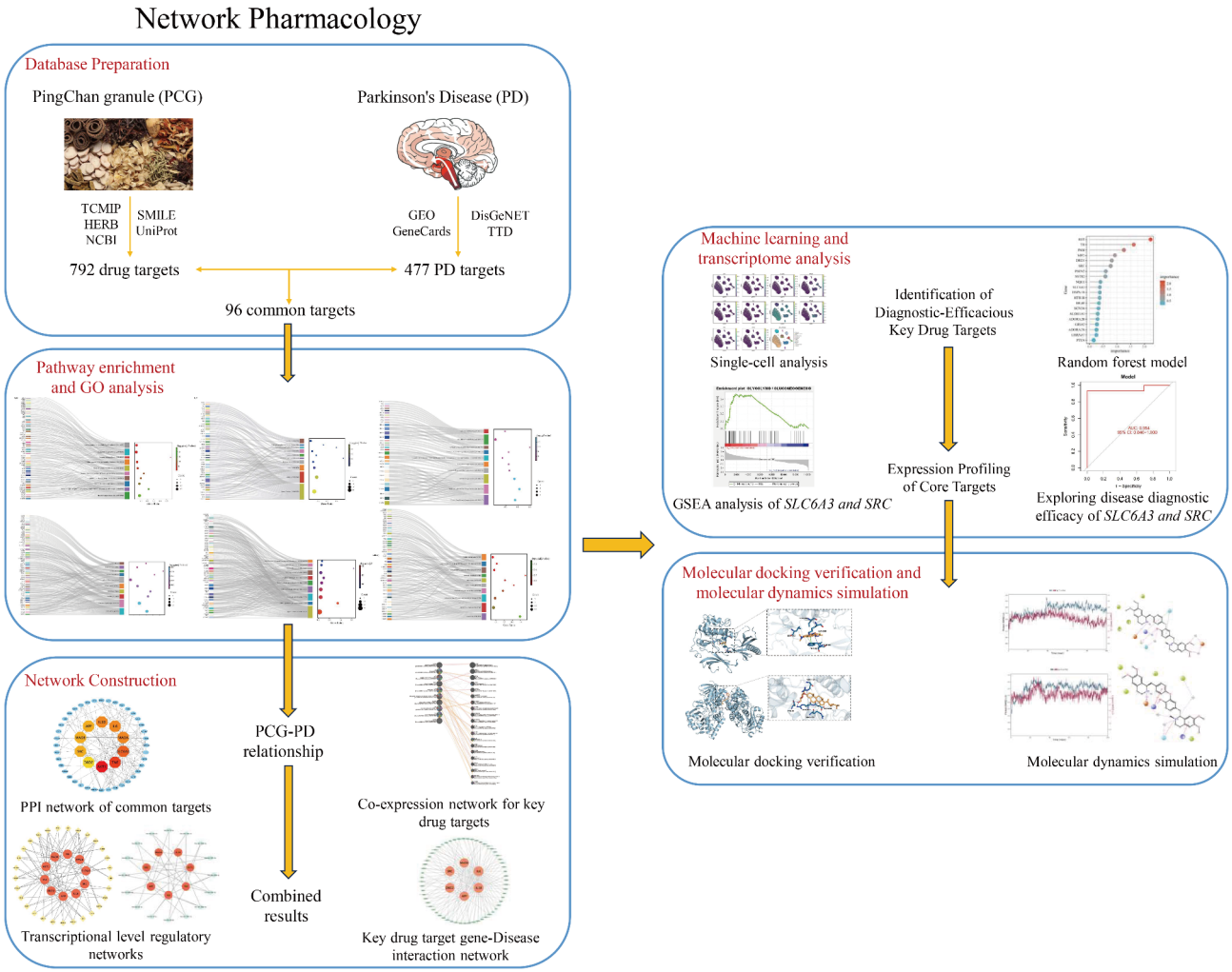

Fig. 1. Pictorial depiction of analytical process used to predict the effect of PCG for PD.

Dataset	Platform	Control	Affected	Total	Source
GSE182622	GPL16791	86	106	192	Dopaminergic neurons
GSE169755	GPL20301	6	6	12	Dopaminergic neurons
GSE20163	GPL96	9	8	17	Substantia nigra
GSE20164	GPL96	5	6	11	Substantia nigra
GSE20292	GPL96	18	11	29	Substantia nigra
GSE7621	GPL570	9	16	25	Substantia nigra
GSE178265	GPL24676	8	7	15	Substantia nigra
GSE157783	GPL24676	6	5	11	Midbrain

Table 1. Details of GEO datasets.

Transcriptome and single-cell nuclei sequencing data collection

To elucidate the molecular mechanisms underlying the pharmacological effects of PCG in PD, we curated bulk RNA-seq and single-nucleus RNA sequencing (snRNA-seq) datasets from the National Center for Biotechnology Information's GEO database (https://www.ncbi.nlm.nih.gov/geo/)[20]. Specifically, we selected the only two available bulk RNA-seq datasets profiling dopaminergic neurons (GSE182622[21] and GSE169755[22]), the four largest substantia nigra transcriptome datasets (GSE20163[22], GSE20164[22], GSE20292[23], and GSE7621[24]), the snRNA-seq dataset with the highest number of dopaminergic neurons (GSE178265[25]), and a comprehensive midbrain snRNA-seq dataset (GSE157783[26]). These datasets provided a robust framework for investigating transcriptional alterations at both the bulk tissue and single-cell levels. A summary of dataset details is presented in Table 1.

Identification of potential target genes

To screen potential target genes, we conducted a meticulous search in the GEO dataset for mRNA expression profiles of dopaminergic neurons in both PD and normal control subjects. Two datasets, GSE182622 (comprising 86 normal control samples and 106 PD patient samples) and GSE169755 (containing 6 normal control samples and 6 PD patient samples), were selected for analysis. Batch effect correction, data normalization, and dispersion estimation were performed using the DESeq2 package in R, following its standard analytical pipeline. Differential gene expression analysis was conducted under stringent criteria (LogFC < -1 or LogFC > 1, adjusted p-value < 0.05) to ensure robust and biologically meaningful results. Simultaneously, single-cell data from the substantia nigra region of the brain were procured through GSE178265 (SCP1768). The provided expression matrix was carefully examined, and corresponding meta-information was recorded. From this dataset, dopamine neuronal cells from individuals with PD and normal controls were identified and selected, encompassing 7 PD samples and 8 normal samples, for advancing our analysis. To address potential batch effects originating from different sample sources, we implemented a "harmony" approach. Our data preprocessing workflow involved linear scaling, normalization using the "LogNormalize" technique, and the identification of highly variant genes using the "vst" method, with parameter settings at "nfeatures = 2000" and "dim.use = 10" to ensure optimal data preparation. A comprehensive visual analysis, guided by the cell grouping results documented in the literature by Tushar Kamath et al.[25], the principal contributor to this dataset, led to the identification of 10 distinct subpopulations of transcriptionally unique DA neurons. Subsequently, The differences in dopaminergic neurons between PD patients and normal controls were assessed using the likelihood-ratio (LR) test, applying stringent thresholds (LogFC < -1 or LogFC > 1, adjusted p-value < 0.05, pct1 > 0.1, pct2 > 0.1) to ensure statistical robustness and biological relevance. Volcano plots for both bulkRNA-seq and snRNA-seq were created using the ggplot2 package in R. Additionally, data on PD-related disease targets were curated from three databases, including the GeneCards database (http://www.genecards.org/)[27], DisGeNET database (https://www.disgenet.org/)[28], and Therapeutic Target Database TTD (http://www.genecards.org/://db.idrblab.net/ttd/)[29], using "Parkinson's disease" as the keyword. A Venn diagram was then drawn to integrate the differentially expressed genes obtained by bulkRNA-seq, snRNA-seq, and potential PD targets from the three databases. Finally, to predict overlapping genes between PCG and PD, a Venn diagram was constructed to retrieve intersecting genes. These overlapping genes were subsequently identified as potential anti-Parkinson targets of PCG.

Functional annotation and pathway analysis

A comprehensive suite of enrichment analyses was executed using the Enrichr tool (https://maayanlab.cloud/Enrichr/)[30] to meticulously unravel detailed insights into biological mechanisms and signaling pathway characteristics. The Gene Ontology (GO) was employed, encompassing three facets: biological process, molecular function, and cellular component. Additionally, Kyoto Encyclopedia of Genes and Genomes (KEGG) pathways were utilized to identify metabolic pathways[31–33]. To ensure a thorough exploration of relevant signaling pathways, the WikiPathways and Reactome databases were integrated with KEGG pathways. This study adopted a stringent criterion of adj.p value < 0.05. The top 10 GO enriched pathways and the top 10 KEGG, WikiPathways, and Reactome pathways with higher counts were selectively chosen for in-depth analysis. Subsequently, the ggplot2 package, provided by R, was employed to visually represent the pivotal pathways.

Construction of protein-protein interaction network and identification of hub targets

The anti-PD targets associated with PCG were input into the STRING database (https://www.string-db.org)[34] for a comprehensive PPI analysis. To ensure the authenticity and accuracy of the data, a high confidence level of 0.7 was chosen as the analysis threshold. Subsequently, the analysis outcomes were imported into Cytoscape 3.9.1 software. Cytoscape 3.9.1 offers a spectrum of 11 distinct topological methods[35]. The degree method was selected to identify hub genes based on connectivity. The degree metric signifies the number of direct neighbors a node has; nodes with a higher degree of connectivity wield greater influence due to their increased number of connections. Additionally, betweenness centrality, representing the number of shortest paths through a node, was considered, with lower values indicating nodes of lesser importance in the network.

Co-expression and functional analysis of hub drug target genes

To unravel the intricate relationships and functions of hub drug target genes, we employed the GeneMANIA algorithm (https://genemania.org/)[36]. This algorithm harnesses diverse data resources encompassing co-expression patterns, genetic interactions, shared protein domains, physical interactions, and co-localization networks. Leveraging these rich datasets, we constructed a predictive gene interaction network specifically tailored to hub drug target genes.

Identifying the relationship of transcription factors and MiRNAs to hub drug targets

Transcription factors (TFs), pivotal proteins that selectively bind to specific genes and regulate the transcription process, play a crucial role in molecular research. Recognizing their significance, we employed the NetworkAnalyst platform[37] to identify topologically significant TFs from the JASPAR database[38] known to bind to our hub drug targets. JASPAR, a publicly available resource, provides comprehensive information on TFs across multiple species in six taxonomic groups. NetworkAnalyst, a robust online platform designed for meta-analysis of gene expression data and the exploration of biological mechanisms, effects, and interpretations, facilitated this investigation. Additionally, we incorporated miRNAs targeting gene interactions to discern miRNAs attempting to bind to gene transcripts and potentially modulate the expression of hub drug target proteins. The mirTarbase[39], a preeminent experimentally validated database of miRNA-gene interactions, was utilized for this purpose. Through NetworkAnalyst, we extracted miRNAs from mirTarbase that interact with hub drug target genes, emphasizing topological analysis in the process. Both the TFs-drug target gene and

miRNAs-drug target gene interaction networks were intricately illustrated using Cytoscape, providing a visual representation of these intricate regulatory relationships.

Hub drug target gene-disease association analysis

DisGeNET stands as a comprehensive database meticulously aggregating gene-disease associations from diverse sources, providing an in-depth characterization of various biomedical dimensions of diseases[28]. This resource is instrumental in unveiling novel insights into human genetic diseases. In tandem, we employed NetworkAnalyst[37] to interface with the DisGeNET database, delving into the intricate relationships between hub drug target genes and diseases. The objective was to discern whether the identified hub drug target genes possess the potential to concurrently address chronic complications associated with PD.

Selecting hub drug target genes through a random forest model and exploring their disease diagnostic efficacy

The GEO database was employed to acquire two RNA-seq datasets of PD substantia nigra, GSE20163 and GSE20164, which were subsequently amalgamated into an internal training set. Additionally, datasets GSE20292 and GSE7621, representing substantia nigra data from PD patients and health controls, were downloaded for use as external validation sets. The array data for GSE20163 corresponds to 8 PD patient samples and 9 control samples, GSE20164 includes 6 PD patient samples and 5 control samples, GSE20292 consists of 11 PD patient samples and 18 control samples, and GSE7621 comprises 16 PD patient samples and 9 control samples. Within the internal training set, a random forest model[40] was meticulously applied to screen the 96 anti-PD drug target genes of PCG. We input the hub gene expression matrix, listing behavioral gene names as sample names, with the outcome variable being binary (PD disease vs. control). The running parameters were: random seed 123,456, 1000 total branches, and ten-fold cross-validation. The output included the overall out-of-bag (OOB) error for each decision and the importance ranking of different genes, based on the descending Gini coefficient. Drug targets with a Gini coefficient exceeding 0.25 were designated as central variables for subsequent analysis. A Venn diagram illustrated the intersection of these central drug targets with the 10 previously identified PPI targets. The intersecting genes were then used to construct a disease diagnosis model via logistic regression in a generalized linear model (GLM)[40]. The "pROC" package was utilized to construct receiver operating characteristic (ROC) curves and calculate area under the curve (AUC) values[41]. Independent validation cohorts GSE20292 and GSE7621 robustly validated the diagnostic efficacy of the central drug targets.

Analysis of midbrain single-cell nuclei sequencing data in PD patients

The snRNA-seq data from midbrains of PD patients were retrieved from GEO (GSE157783), encompassing 5 midbrain samples from PD patients[26]. Genes expressed in fewer than three cells or cells expressing fewer than 200 genes were excluded during the data preprocessing step. Quality control measures were further implemented based on the counting matrix, considering the number of genes expressed and the percentage of mitochondrial gene counts in each cell. Cells with total counts exceeding 25,000 underwent library size correction using the "scanpy.pp.normalize_total" function in Scanpy. Logarithmically normalized data matrices were employed for subsequent analyses. Dimensionality reduction and unsupervised clustering were performed using the Scanpy workflow. The "scanpy.pp.highly_variable_genes" function selected the top 4,000 highly variable genes for downstream analysis. To mitigate the impact of total counts per cell and the percentage of mitochondrial genes expressed, the "scanpy.pp.regress_out" function was applied. Gene scaling to unit variance was achieved using "scanpy.pp.scale" with a parameter "max_value = 10". Following data preprocessing, principal component analysis (PCA) was conducted to reduce dimensionality. To address batch effects across different datasets, the "sc.external.pp.harmony_integrate" method with the parameter "n_pcs = 40" was employed. Additionally, the batch effect of the merged dataset was reduced using "scanpy.tl.umap" to visualize the neighborhood graph dimension. The Leiden clustering method was then applied to cluster cells, revealing distinct cell groups such as dopaminergic neurons, microglia, astrocytes, oligodendrocytes, OPCs, CADPS2 + neurons, endothelial cells, pericytes, ependymal cells, excitatory cells, inhibitory cells, and GABAergic cells. To effectively illustrate the hub drug targets within these 12 cell populations, the FeaturePlot function was utilized to create informative plots depicting the distribution.

To delve more profoundly into the alterations in downstream signaling pathways consequent to changes in the expression of SLC6A3 and SRC genes in dopaminergic neurons, we extracted the expression matrix of midbrain dopaminergic neurons. Subsequently, we conducted a correlation analysis between each gene and the gene of interest (SLC6A3 or SRC). The correlation values obtained were then utilized for enrichment analysis, identifying a range of a priori defined biological processes. The background gene set for this analysis was sourced from the KEGG database. Enriched pathways were organized based on normalized enrichment scores, and pathways with a significance level of $P < 0.05$ were earmarked for further analysis.

Molecular docking verification

To validate molecular interactions, all active compounds targeting the 10 hub drug targets underwent a docking process with the respective hub targets. Prior to docking, the receptor underwent preprocessing, involving procedures such as combining non-polar hydrogen, merging charges, eliminating lone pairs of electrons, and removing solvent molecules in proximity to the binding site. Subsequently, the autodock program[42] was employed to conduct semi-flexible docking, generating diverse conformational orientations. This process allowed for the exploration of electrostatic and van der Waals interactions between the ligand molecule and the binding site. Binding energy scores were calculated and visualized as a heatmap, and a subset of conformations with superior scores was selected for visualization using PyMOL[43]. The information files for hub drug targets,

ligands, and detailed docking results from this study are available in the public database at https://doi.org/10.7910/DVN/GCF1Q1.

Molecular dynamics simulation

Following the molecular docking simulations, dauricine exhibited a low binding energy with SLC6A3 and SRC, two hub drug targets demonstrating robust diagnostic performance. Subsequent molecular dynamics simulations involving dauricine and SRC, as well as dauricine and SLC6A3, were conducted using the "Desmond" module within the Schrödinger 2019 software.The simulation employed the predefined SPC water model, and the OPLS2005 force field was utilized for water molecule simulations. To neutralize the system charge, an appropriate quantity of chloride ions/sodium ions was added to balance the system charge, randomly placed within the solvation system. Following the construction of the solvated system, energy minimization was executed using the default protocol integrated with the Desmond module, employing OPLS 2005 force field parameters. Maintaining a temperature of 300 K and 1 atmosphere pressure was achieved through Nose-Hoover temperature coupling and isotropic scaling. Subsequently, an NPT simulation was conducted for 100 ns, saving trajectory data at 100 ps intervals for further analysis. Detailed molecular dynamics simulation result files are accessible in the public database at https://doi.org/10.7910/DVN/GCF1Q1.

Drug target screening via summary-data-based mendelian randomization

Genetic information related to PD was sourced from the finngen_R10_G6_PARKINSON dataset in the Finngen database (https://www.finngen.fi/en) and its associated eQTLGen. To further validate the identified drug targets, we conducted a summary-data-based mendelian randomization (SMR)[44], focusing on targets with significant results. We used expression quantitative trait loci (eQTL) data linked to relevant genes as proxies for PD. Our study employed cis-eQTL as instrumental variables, applying a significance threshold of $p < 5 \times 10\text{^}-8$ and a linkage disequilibrium (LD) cutoff of r^2 < 0.1. The heterogeneity in dependent instruments (HEIDI) test was utilized to assess the LD structure associated with specific SMR loci. This test aims to determine whether there is a difference in the SMR effect estimate between the top eQTL of a specific probe and the variants in its LD, thereby distinguishing linkage-based associations from potential pleiotropic or causal relationships. HEIDI P values below 0.05 were considered significant, indicating the presence of linkage-based SMR associations.

Results

Active compounds and potential targets of PCG

PCG comprise six Chinese herbal medicines—Gou Qi Zi, Sang Ji Sheng, Tian Ma, Shao Yao, Tian Nan Xing, and E Shu—each containing 204, 153, 586, 92, 53, and 101 drug targets, respectively. Additionally, Jiang Can, Quan Xie, and Wu Gong contain 195, 163, and 192 drug targets, respectively (Fig. 2a). Following redundancy elimination, 96 unique compounds were identified. Through searches in the TCMSP and Swiss target prediction databases, we identified 792 potential targets for the active compounds in PCG, along with their corresponding gene symbols (see Supplementary Table S1 for detailed drug-compound-target information).

To explore potential disease treatment targets, we analyzed gene expression levels in PD patient dopaminergic neuron samples and normal control dopaminergic neuron samples. Examination of dopaminergic neuron bulkRNA-seq data (GSE182622 and GSE169755) revealed population differences between the two datasets, as illustrated by PCA results (Fig. 2b). Batch effects were corrected using the Deseq2 package, and differential expression analysis was conducted with criteria set at |logFC| > 1 and adj.$P < 0.05$, resulting in 155 differentially expressed genes—90 up-regulated and 65 down-regulated (Fig. 2c). Furthermore, analysis of single-cell nuclei sequencing results from the substantia nigra of PD patients and normal controls revealed 10 subgroups of dopaminergic neurons, with 7 PD patients contributing 2715 dopaminergic neurons (Fig. 2d), and 8 normal controls contributing 15,648 dopaminergic neurons (Fig. 2e). Differential expression analysis of dopaminergic neurons in PD patients and normal controls (|logFC| > 1, adj.$P < 0.05$, pct1 > 0.1, pct2 > 0.1) identified 12 up-regulated genes and 10 down-regulated genes(Fig. 2f).

Ultimately, we amalgamated disease targets sourced from GeneCards (genes with scores exceeding 50), DisGeNET (genes with gene-disease association scores surpassing 0.1), and TTD. Additionally, we incorporated GEO DEGs, meticulously eliminating any duplicate entries in the process. This comprehensive approach yielded 477 disease targets in PD (Fig. 2g). The intersection of PCG's active compound targets and PD's disease targets identified 96 common targets (Fig. 2h), selected as hub targets for assessing PCG's anti-PD activity.

Pathway enrichment and gene ontology analysis

To delve deeper into the molecular mechanism underlying PCG's therapeutic impact on PD, we conducted comprehensive GO enrichment analysis and explored KEGG, WikiPathway, and Reactome enrichments pertaining to the 96 anti-PD targets associated with PCG. The results were visually represented using a Sankey bubble chart, highlighting the top ten most significant pathways, each with an adjusted P-value of less than 0.05.

The GO enrichment analysis yielded three distinct categories: Fig. 3a illustrates Biological Process (BP), Fig. 3b represents Molecular Function (MF), and Fig. 3c outlines Cellular Component (CC) enrichments for PCG's drug targets. Notably, the top 10 GO terms ranked by BP predominantly relate to neuronal synaptic signaling. Moreover, they exhibit involvement in G protein-coupled receptor signaling pathways, apoptosis-related pathways, and dopamine metabolism pathways. The CC results signify associations with neuronal cytoplasm and synaptic function, while the MF analysis underscores participation in G protein-coupled receptor signaling pathways and neuronal synaptic signal transmission pathways.

Examining the KEGG pathway analysis results (Fig. 3d), the 96 drug targets primarily enrich pathways such as the cAMP signaling pathway, dopaminergic synapse, serotonin synapse, and other pertinent pathways. Consistent findings were observed in Reactome and WikiPathway enrichment analyses (Fig. 3e, f), underscoring

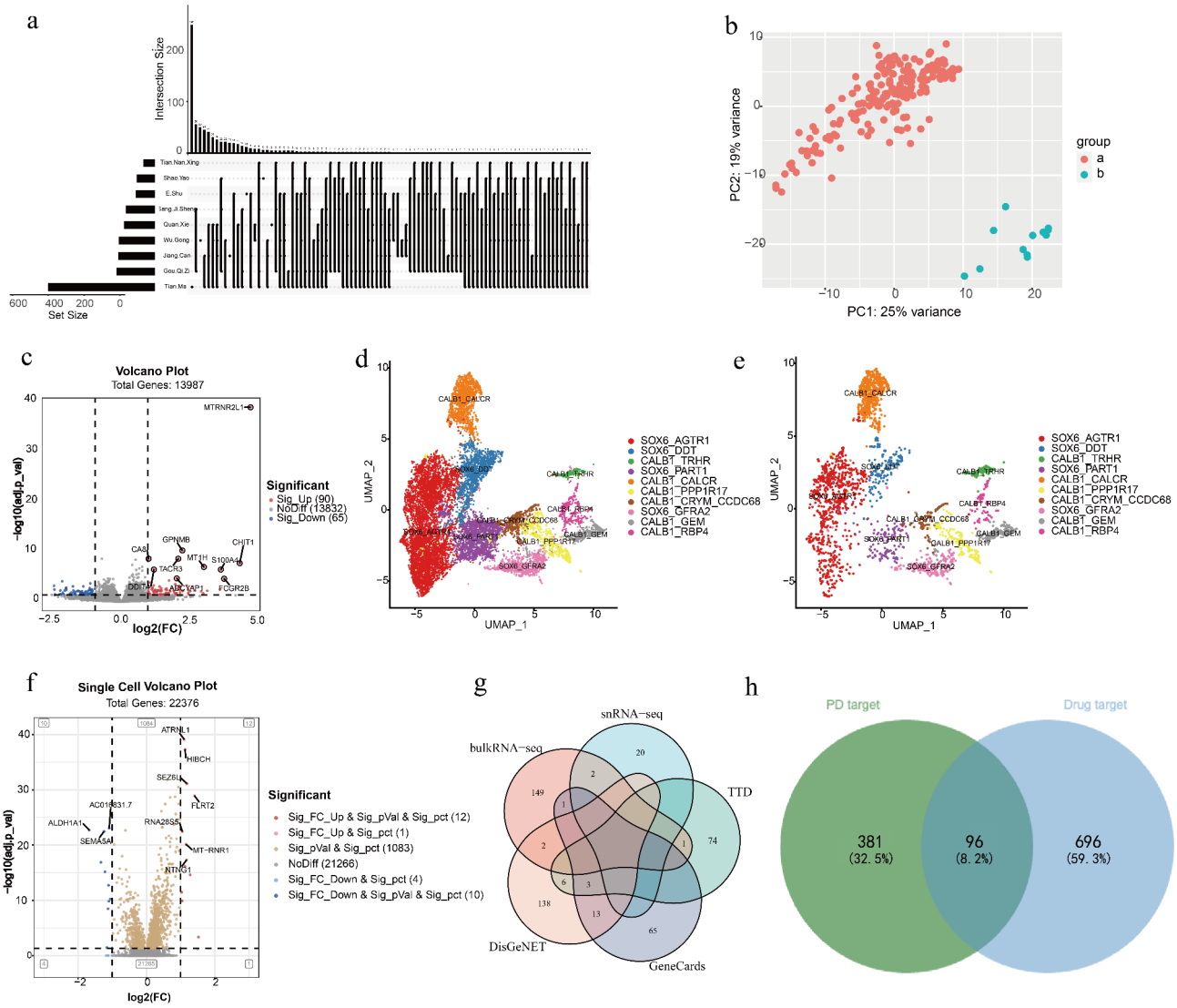

Fig. 2. Identification of Anti-PD Targets of PCG. (**a**) Upset diagram illustrating the distribution of active compounds within each traditional Chinese medicine and Chinese medicinal material in PCG. (**b**, **c**) Principal component analysis diagram of dopaminergic neuron bulkRNA-seq (GSE182622 and GSE169755). Volcano plot showcasing the distribution of differentially expressed genes after addressing batch effects. (**d**) Single-cell nuclei sequencing umap diagram depicting dopaminergic neurons in normal controls. (**e**) Single-cell nuclei sequencing umap diagram representing dopaminergic neurons in PD patients. (**f**) Volcano plot illustrating differentially expressed genes identified through single-cell nuclear sequencing of dopaminergic neurons in PD and healthy controls. (**g**) Venn diagram integrating differentially expressed genes from bulkRNA-seq and single-cell nuclear sequencing, along with PD treatment targets sourced from the TTD, DisGeNET, and GeneCards databases. (**h**) Venn diagram revealing the intersection of 96 common targets shared between PCG active compound targets and PD disease targets.

the impact of these drug targets on intercellular signal transduction, synaptic signaling, and G protein-coupled receptors.

PPI network analysis identifies hub drug targets, constructs transcriptional level regulatory networks, and identifies disease associations

To decipher the therapeutic mechanism of PCG in PD, we inputted 96 drug targets into the STRING database to construct a PPI network, consisting of 96 nodes and 171 edges. Utilizing the degree algorithm in Cytoscape's cytoHubba package, we identified the top 10 (10.4%) drug targets as the most influential, visually represented in Fig. 4a. The color depth of a hub drug target denotes its degree of interconnectedness; heightened connections indicate greater significance. The top 10 most influential drug targets include *AKT1*, *TNF*, *SLC6A3*, *MAOA*, *IL1B*, *IL6*, *APP*, *MAOB*, *SRC*, and *DRD2*, with detailed information in Table S2.

Next, we employed the GeneMANIA website to construct a co-expression network for these hub drug targets (Fig. 4b). Within the complex PPI network, co-expression interactions accounted for 30.35%, physical

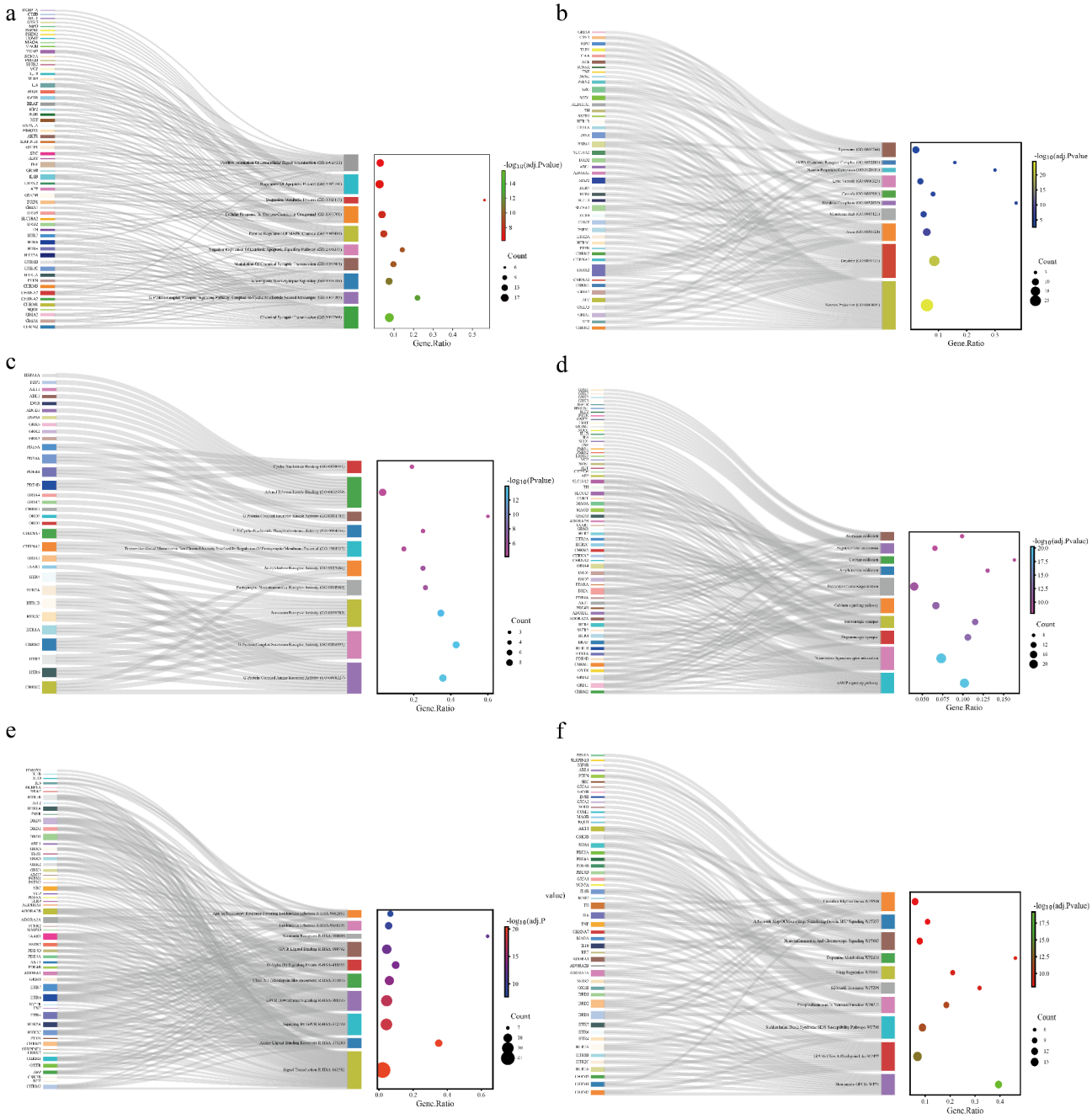

Fig. 3. Functional and Pathway Enrichment Analyses of Anti-PD Targets of PCG. (**a**) Biological process analysis. (**b**) Molecular function analysis. (**c**) Cellular component analysis. (**d**) KEGG pathway analysis. (**e**) Reactome pathway analysis. (**f**) WikiPathway analysis.

interactions for 36.54%, co-localization for 3.04%, predicted interactions for 28.47%, and shared protein domains for 3.34%. Functional analysis highlighted their involvement in processes such as the neuroinflammatory ERBB signaling pathway.

To delve deeper into hub drug target genes and identify potential transcriptional level regulation after changes in drug targets, we utilized a network-based approach to unravel regulatory TFs and miRNAs. The drug target gene-TFs interaction network, as shown in Fig. 4c, illustrates drug target genes represented by circles and TFs by diamonds. The degree of a TF node indicates its level of connection within the network, with higher degrees signifying greater importance. Noteworthy TFs include FOXC1, GATA2, TFAP2A, YY1, and HINFP. Furthermore, Fig. 4d depicts the interaction of miRNA regulators with hub drug target genes. Our findings underscore the significance of hsa-mir-106a-5p, hsa-mir-34a-5p, and hsa-mir-203a-3p as central hubs in the miRNA-drug target gene interaction network.

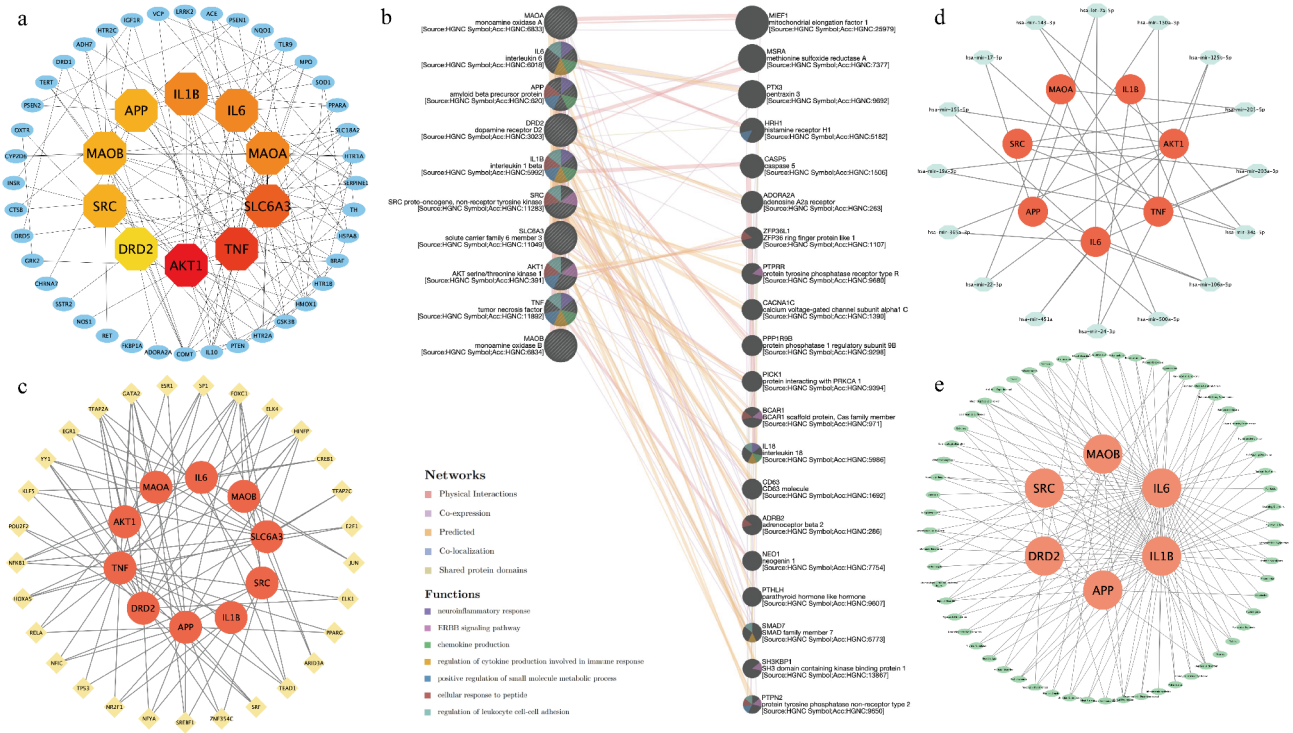

Fig. 4. Network-Based Identification and Functional Analysis of Hub Drug Targets of PCG in PD (**a**) Interaction network of PCG anti-PD targets and extraction of hub drug targets. (**b**) Functional network of hub drug targets generated by GeneMANIA. (**c**) Regulatory network illustrating the interactions between hub drug targets and transcription factors. (**d**) Regulatory network depicting the interactions between hub drug targets and microRNAs. (**e**) Interaction network demonstrating the connections between hub drug targets and the disease.

Considering the shared genetic components between PD and related diseases, our strategy involved deciphering the relationship between drug target genes and diseases. Gene-disease association analysis on the DisGeNET platform suggested that PCG may effectively ameliorate depression, bipolar disorder, and related mental health disorders by acting on these hub drug targets. These conditions are frequently associated with Parkinson's patients, corroborated by previous clinical randomized controlled trials demonstrating PCG's efficacy in alleviating depression in PD patients. Moreover, the target gene-disease association network diagram hinted at the potential concurrent improvement in cerebral ischemia, epilepsy, schizophrenia, and other related neurological diseases through PCG acting on these hub drug targets (Fig. 4e). However, comprehensive validation of these potential benefits necessitates further scrutiny through rigorous clinical and foundational experiments.

Screening core drug targets using random forest models and exploring potential diagnostic efficacy with generalized linear models

The substantia nigra exhibits the most pronounced pathological changes in PD patients. Differentially expressed genes in this region are critical to PD pathogenesis and may serve as potential therapeutic targets. Thus, we conducted a comprehensive analysis of transcriptome data from the substantia nigra to evaluate the expression changes of core drug targets in PD patients and explore their potential as diagnostic biomarkers. We extensively searched the GEO database and obtained four substantia nigra RNA-seq datasets, including normal controls and primary PD patients: GSE20163, GSE20164, GSE7621, and GSE20292. In datasets GSE20163 and GSE20164, we applied a random forest model to examine the expression of 96 anti-PD drug targets from PCG. This analysis aimed to identify genes associated with disease pathogenesis and determine core drug targets. We screened the top 17 key drug targets from the variable pool, considering those with a Gini coefficient greater than 0.25 (Fig. 5a). Subsequently, a Venn diagram depicted the intersection of these 17 drug targets with the 10 core targets identified in the PPI network, highlighting two drug target genes as potential biomarkers in the substantia nigra of PD with promising therapeutic prospects (Fig. 5b).

To delve into the predictive value of these two hub genes for PD, specifically *SLC6A3* and *SRC*, we conducted ROC analysis in the training set (Fig. 5c). The ROC analysis indicated robust diagnostic performance, with an AUC of 0.949 for SLC6A3 and 0.826 for *SRC*. Further analysis involved utilizing the expression of these two genes from the training set to construct a PD disease diagnosis model through a generalized linear model, affirming their commendable diagnostic efficacy (AUC = 0.954) (Fig. 5d). This diagnostic performance was consistently validated in two independent cohorts, GSE7621 and GSE20292, with AUC values of 0.910 (Fig. 5e) and 0.838 (Fig. 5f), respectively.

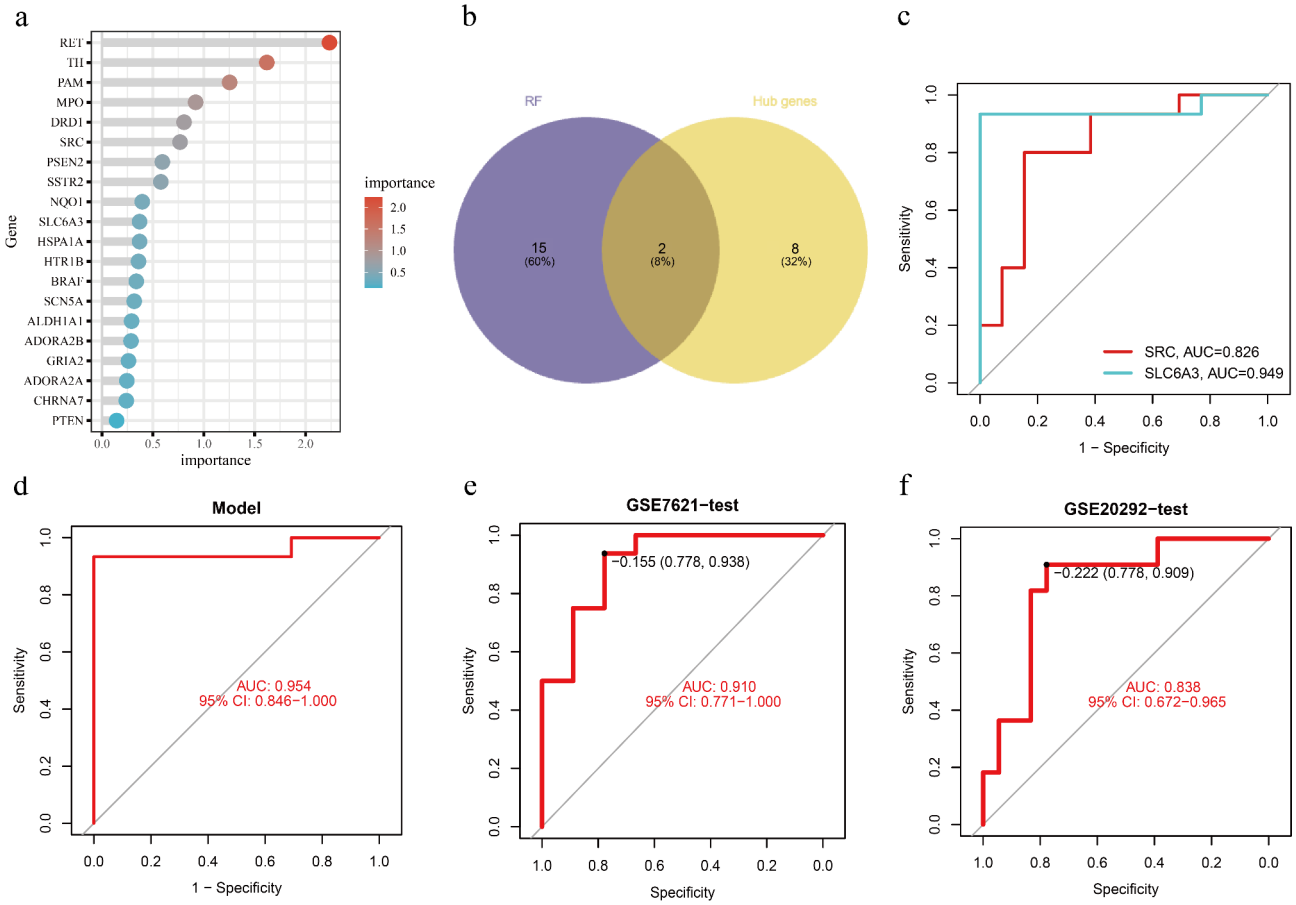

Fig. 5. Screening and Validation of Hub PCG Anti-Parkinson's Targets with Diagnostic Potential (**a**) Feature importance ranking generated by random forest modeling of 96 drug target genes derived from substantia nigra transcriptome data. (**b**) Venn diagram analysis showcasing the intersection of the 17 hub genes identified through random forest and the 10 hub drug target genes from the previous PPI network. (**c**) ROC curve illustrating the diagnostic performance of two hub drug target genes in the training set model. (**d**) ROC curve portraying the performance of the GLM in the training set model construction, focusing on the two hub drug target genes. (**e**) ROC curve for the independent validation set GSE7621. (**f**) ROC curve for the independent validation set GSE20292.

Outcome	probeID	Gene	topSNP	OR(95% CI)	P_SMR	P_HEIDI
Pakinsonism						
	ENSG00000197122	SRC	rs6017916	2.20 (1.09 to 4.46)	0.028	0.308

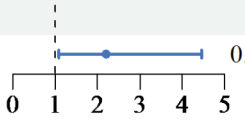

Fig. 6. SMR Analysis of PD. Forest plot illustrating the SMR analysis results, demonstrating the association between *SRC* and PD.

Mendelian randomization analysis of hub anti-PD targets of PCG

MR analysis identified *SRC* as a promising candidate drug target for PD. The odds ratio (OR) for SRC was 2.20 (95% CI: 1.09 to 4.46, $p = 0.028$), with P_HEIDI = 0.308, as depicted in the forest plot (Fig. 6). Additionally, the scatter plot (Supplementary Fig. 1) illustrated the relationship between the eQTL and GWAS effect sizes of the SRC gene, supporting the MR findings by showing a consistent relationship between these effect sizes. These combined analyses strongly indicate that *SRC* is a significant risk factor for PD, highlighting the therapeutic potential of PCG through its action on the *SRC* drug target to mitigate the disease.

Expression profiling of hub targets across midbrain cell types

To gain deeper insights into the differential expression patterns of hub targets within various midbrain cell types, we scrutinized the cell composition of PD patient midbrain tissue and assessed the expression of the 10 hub

targets through single-cell nuclei sequencing analysis. Illustrated in Fig. 7a-b, we classified 12 distinct cell types based on marker genes and prior research[26]: dopaminergic neurons, microglia, astrocytes, oligodendrocytes, OPCs, CADPS2 + neurons, endothelial cells, pericytes, ependymal cells, excitatory cells, inhibitory cells, and GABAergic cells.

Among these cell types, *SLC6A3* exhibited high expression primarily in dopaminergic neurons, while *SRC* manifested expression in dopaminergic neurons, excitatory neurons, inhibitory neurons, and pericytes. Notably, APP and AKT1 displayed ubiquitous expression across all cell types. Furthermore, TNF, IL1B, and IL6 demonstrated notably lower expression levels across various cell types. DRD2 predominantly expressed in dopaminergic neurons, and MAOB exhibited widespread expression in dopaminergic neurons, excitatory neurons, inhibitory neurons, astrocytes, and epithelial cells. (Fig. 7c) This comprehensive analysis sheds light on the nuanced distribution of hub target expression within distinct midbrain cell populations, providing valuable insights into the potential therapeutic impact of these targets on specific cell types in the context of PD.

To further scrutinize the widely distributed hub drug targets, *SLC6A3* and *SRC*, in dopaminergic neurons and comprehend the effects of their gene expression changes on potential pathways in dopaminergic neurons, we conducted correlation analysis between each gene in every dopaminergic neuron in the midbrain single-cell sequencing set and the hub drug target gene (*SLC6A3* or SRC). The resulting correlation values were employed for gene set enrichment analysis (GSEA). We postulate that Dauricine, the active compound in PCG, acts on *SLC6A3*, a hub drug target in dopaminergic neurons, potentially modulating the mitophagy pathway (Fig. 7d), synaptic vesicle cycle pathway (Fig. 7e), glycolysis/gluconeogenesis pathway (Fig. 7f), thereby playing a protective role in dopaminergic neurons. Similarly, Dauricine may influence the phosphoinositide metabolism pathway in dopaminergic neurons (Fig. 7g), the pentose phosphate pathway (Fig. 7h), and the NF-KAPPA B signaling pathway (Fig. 7i), contributing to neuroprotection.

Molecular docking for validation

To validate the findings from network pharmacology, we employed molecular docking techniques to assess the binding affinities between identified compounds and hub targets. Utilizing degree values obtained from the Protein-Protein Interaction (PPI) network, we meticulously selected 10 hub drug targets along with their corresponding 23 compounds for an exhaustive molecular docking analysis. The resulting distribution of docked binding energies is visually represented in the form of a heat map (Fig. 8a). Lower binding energies indicate stronger binding activity between the ligand and the receptor protein. Generally, an affinity energy greater than − 5 kcal/mol suggests no predicted binding, an affinity energy less than − 5 kcal/mol indicates moderate predicted binding, and an affinity energy less than − 7 kcal/mol indicates strong predicted binding, as established in previous studies[45]. Notably, for SLC6A3, SRC, AKT1, MAOA, and MAOB, the active compounds in PCG exhibited docking binding energies lower than − 7 kcal/mol, signifying their potential as binding targets for these active compounds.

Furthermore, detailed visualization studies were conducted using PyMoL and Discovery Studio, focusing on four pairs of compound-target interactions with free binding energies less than − 10 kcal/mol. Additionally, examination was extended to include the hub drug target SLC6A3 and the active compound dauricine, resulting in a total of five pairs (Fig. 8b-f). Specific docking scores, key residues involved, and bond types for these interactions are detailed in Supplementary Table 3. The free binding energies within the docking results ranged from − 8.2 to − 10.4 kcal/mol, underscoring the stability of these binding interactions. This meticulous molecular docking analysis serves to not only validate but also enrich our understanding of the potential binding potency of selected compounds to hub drug targets, thereby unraveling the intricate molecular mechanisms that underlie their therapeutic efficacy.

Molecular dynamics simulation

To substantiate the binding efficacy of small molecule compounds with hub target proteins, molecular dynamics simulations were conducted, focusing on those exhibiting the most favorable binding abilities in molecular docking. Dauricine's interaction with SLC6A3 proteins and its interaction with SRC were specifically chosen for molecular dynamics simulations. These target proteins underwent significant alterations in the substantia nigra of PD patients, demonstrating robust diagnostic performance and pivotal roles in PD development. Notably, during molecular docking, these interactions displayed formidable binding forces, measuring − 8.2 kcal/mol and − 10.2 kcal/mol, respectively. The ensuing molecular dynamics simulations aim to provide a dynamic perspective on the stability and behavior of these interactions, further elucidating their potential therapeutic impact on PD.

Molecular dynamics simulations stand as a widely embraced methodology, offering insights into the structural properties of protein-ligand systems and shedding light on the binding stability between proteins and ligands. In our study, a meticulous 100 ns molecular dynamics simulation of dauricine with SLC6A3 (Fig. 9) and SRC (Fig. 10) provided a detailed glimpse into the interactions unfolding within the active domain of the proteins. These interactions were characterized by water bridges, hydrophobic interactions, and hydrogen bonding, collectively forming robust connections that significantly contributed to understanding the overall stability of the binding.

Upon completion of the simulation, hub parameters such as the root mean square deviation (RMSD) and root mean square fluctuation (RMSF) of the protein-ligand complex system were meticulously calculated. In the case of dauricine and SLC6A3 simulations, the RMSD of the free protein exhibited an initial increase, followed by fluctuations around 2.3 Å after 5 ns and approximately 2.8 Å after 40 ns. Interestingly, protein RMSD fluctuations consistently remained within 3.0 Å for the majority of the simulation, maintaining a stable value, indicative of simulation convergence (left axis of Fig. 9a). The ligand exhibits fluctuations ranging from 1.8 to 2.4 Å (right axis of Fig. 9a), with the majority of values not surpassing the observed protein RMSD. This observation indicates that the ligand effectively maintains its position without diffusing from its initial binding site, thereby

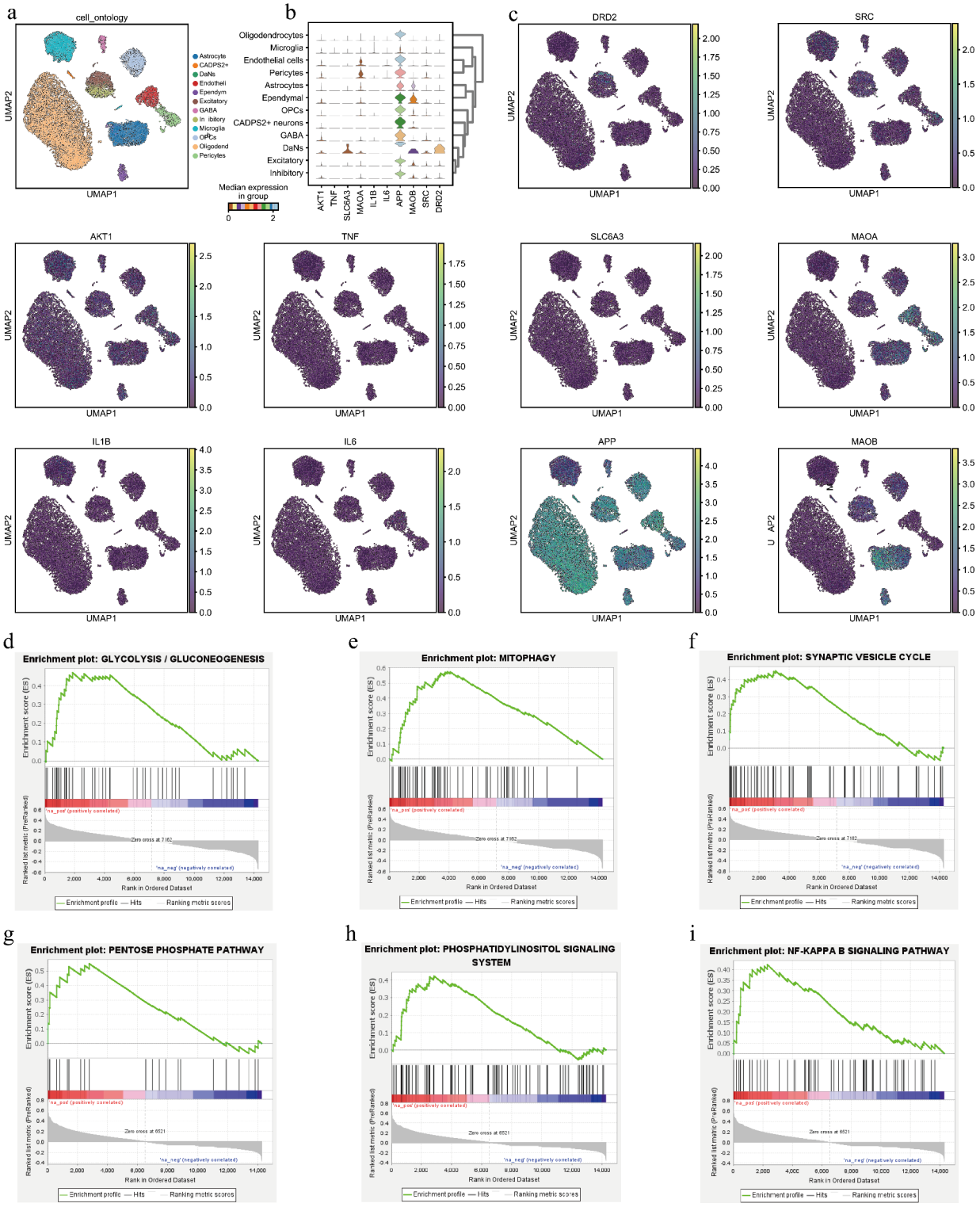

Fig. 7. Cellular Expression and Functional Insights of Hub Drug Target Genes in the Midbrain (**a**) Uniform Manifold Approximation and Projection (UMAP) plot delineating 12 distinct cell clusters (**b**) Violin plot illustrating the distribution of the 10 hub drug target genes across the 12 different cell types. (**c**) Expression patterns of hub drug targets within various cell types. Gene Set Enrichment Analysis (GSEA) of the *SLC6A3* single gene in dopaminergic neurons revealed significant alterations in: (**d**) Glycolysis/Gluconeogenesis Pathway, (**e**) Mitophagy Pathway, and (**f**) Synaptic Vesicle Recycling. Similarly, single-gene GSEA analysis on SRC in dopaminergic neurons uncovered changes in: (**g**) Pentose Phosphate Pathway, (**h**) Phosphoinositide Metabolism, and (**i**) NF-Kappa B Signaling Pathway.

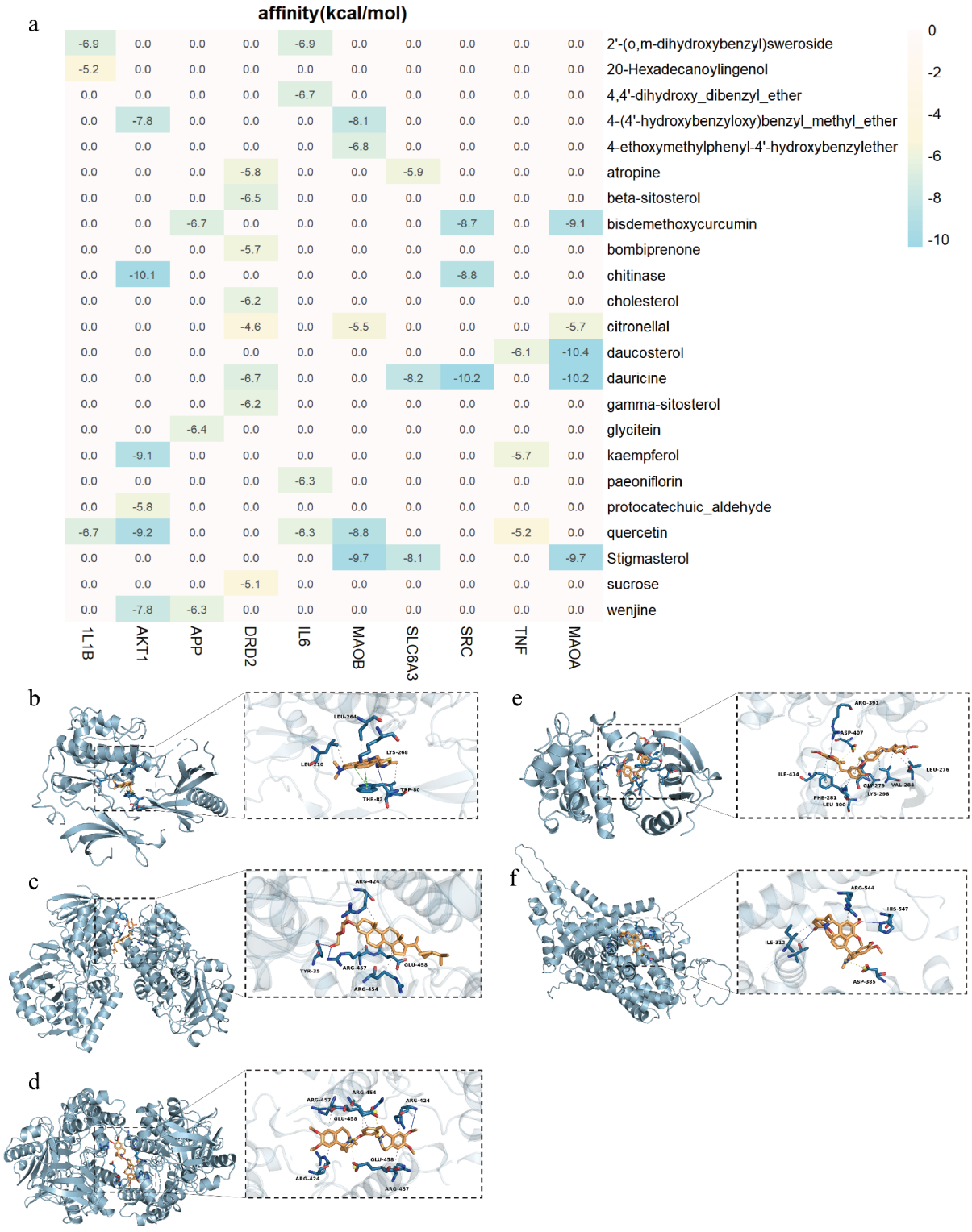

Fig. 8. Molecular Docking Simulations Between PCG Active Compounds and Hub Drug Targets (**a**) Docking heat score depicting the interaction between hub targets and active compounds. (**b**) Chitinase-AKT1 docking simulation. (**c**) Daucosterol-MAOA docking simulation. (**d**) Dauricine-MAOA docking simulation. (**e**) Dauricine-SRC docking simulation. (**f**) Dauricine-SLC6A3 docking simulation.

suggesting the attainment of a metastable state for the protein complex during the 100 ns simulation. Similarly, in the molecular dynamics simulations of dauricine and SRC, the RMSD of the free protein experienced an initial increase, stabilizing around 2.8 Å after 20 ns, indicating convergence (Fig. 10a, left axis). Concurrently, the ligand demonstrated fluctuations in the range of 2.0 Å to 3.0 Å for the majority of the simulation (Fig. 10a,

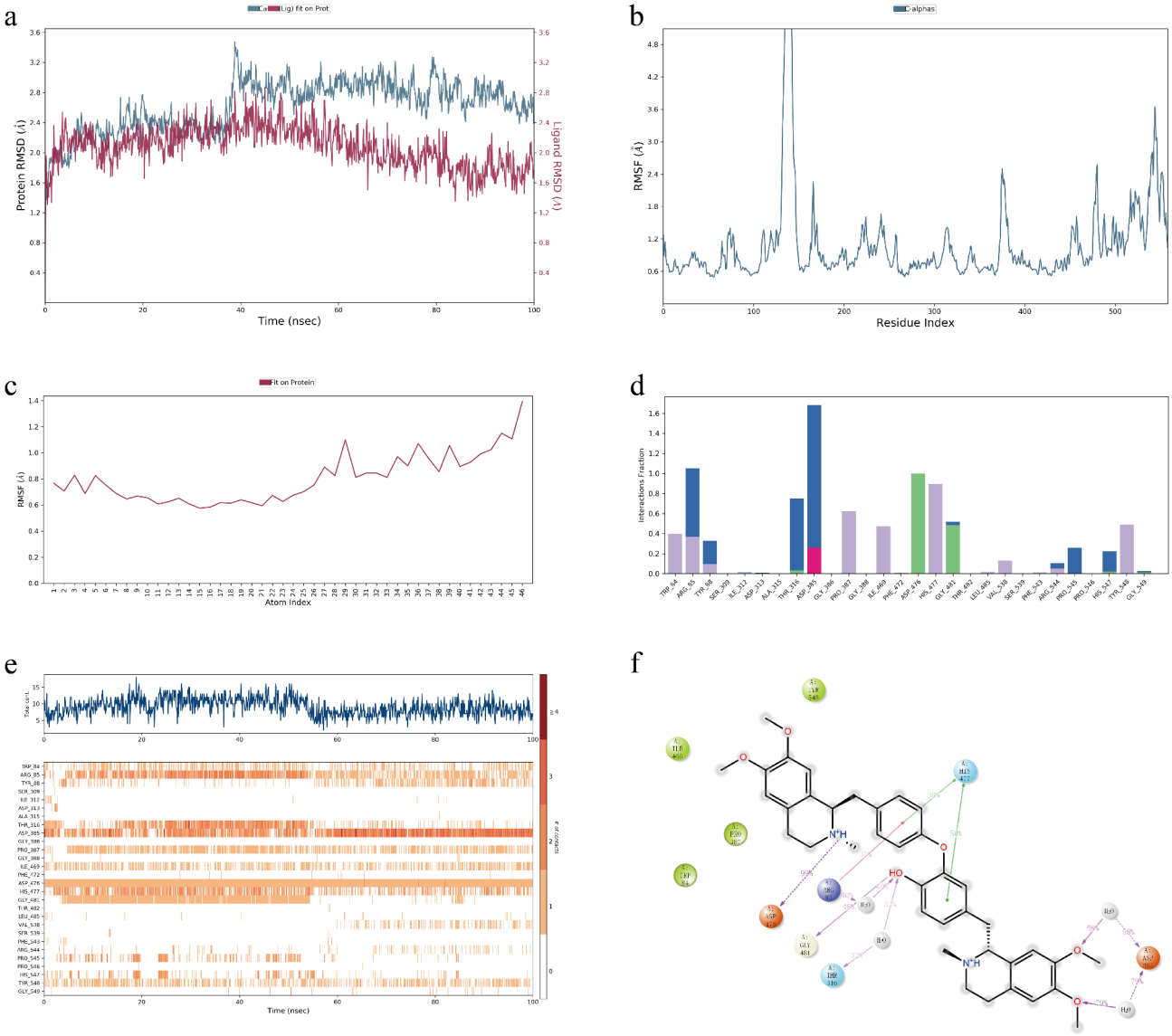

Fig. 9. Molecular dynamics simulation using SLC6A3 protein and dauricine. (**a**) Root mean square deviation (RMSD) plots of C-α atoms of SLC6A3 and dauricine are displayed. The SLC6A3 trajectory is depicted by the green line, while the dauricine trajectory is represented by the red line. The left Y-axis denotes the RMSD of SLC6A3, and the right Y-axis represents the RMSD of dauricine aligned with the protein. The X-axis indicates simulation time in nanoseconds. (**b**) Root mean square fluctuation (RMSF) plot of C-α atoms of SLC6A3. (**c**) RMSF plot of dauricine. (**d**) Fractional interaction (occupancy) plot of SLC6A3 with dauricine. The Y-axis illustrates the total number of contact fractions for each residue at each simulation time. For instance, if a residue (indicated on the X-axis) maintains a single contact throughout the entire 100 ns simulation, its interaction score will be 1. Notably, ASP 385 has a score of approximately 1.7, indicating that it retains at least 1 contact point throughout the simulation. (**e**) Protein-ligand interactions (H-bonds, hydrophobic, ionic, water bridges) are represented along a time axis. (**f**) Protein-molecule interactions and hydrogen-bonding interactions are depicted by purple arrows.

right axis), further supporting the notion of the protein complex reaching a metastable state during the 100 ns simulation.

Furthermore, we meticulously recorded the fluctuations of amino acid residues interacting with dauricine in SLC6A3 and SRC through protein root mean square fluctuation (RMSF) plots (Figs. 9b and 10b). The ligand RMSF plots illuminated atomic-scale fluctuations of the ligand (Figs. 9c and 10c), offering a nuanced understanding of the interaction dynamics between ligand fragments and proteins, emphasizing their entropic role in binding events. Throughout the simulation, the interactions between dauricine and SLC6A3, as well as dauricine and SRC, were diligently monitored and categorized by type, encapsulating hydrogen bonds, hydrophobic bridges, ionic bridges, and water bridges (Figs. 9d and 10d). These interactions were further visualized through stacked

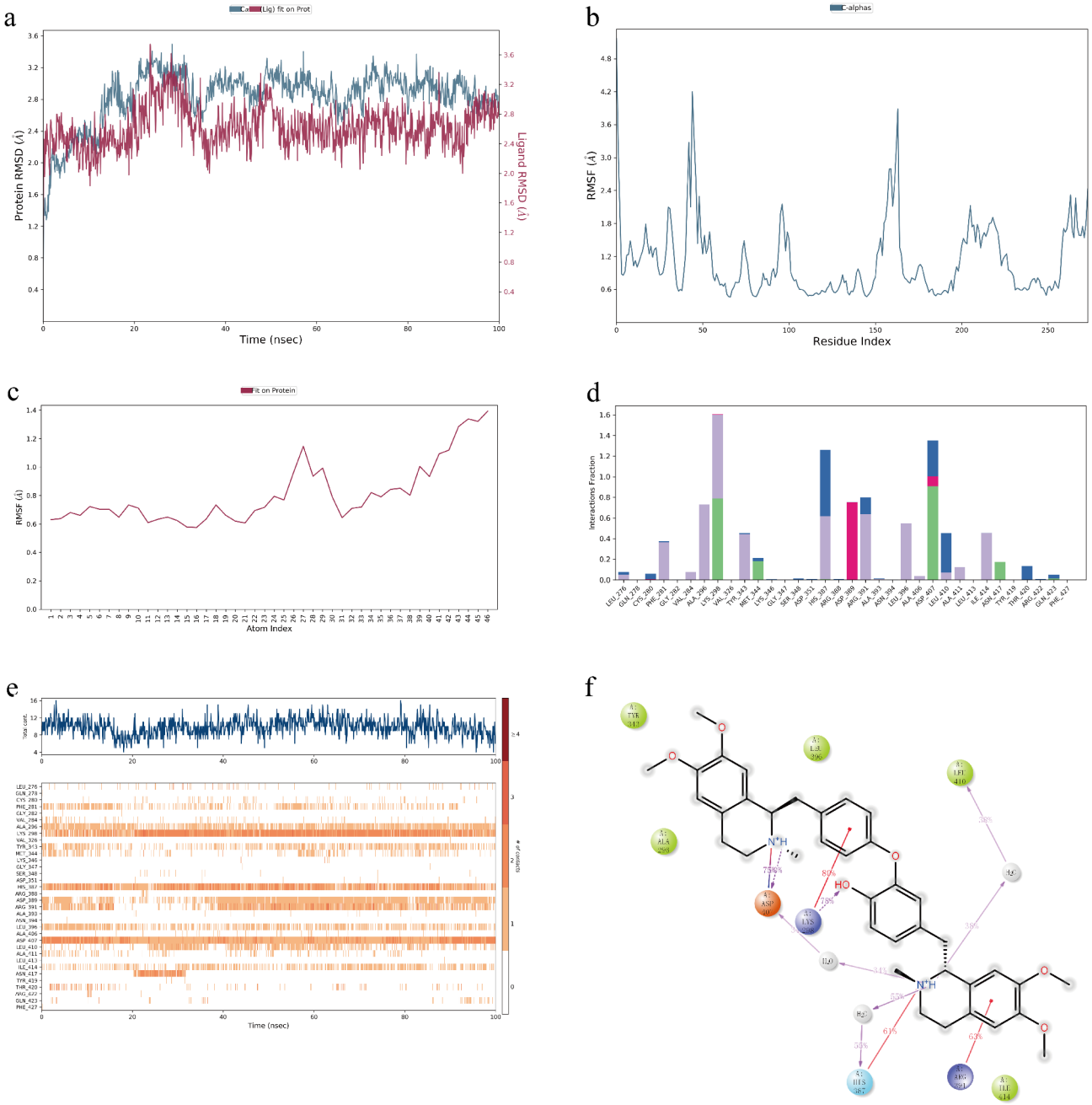

Fig. 10. Molecular dynamics simulation using SRC protein and dauricine. (**a**) RMSD plots of C-α atoms of SRC and dauricine are displayed. The SRC trajectory is depicted by the green line, while the dauricine trajectory is represented by the red line. The left Y-axis denotes the RMSD of SRC, and the right Y-axis represents the RMSD of dauricine aligned with the protein. The X-axis indicates simulation time in nanoseconds. (**b**) RMSF plot of C-α atoms of SRC. (**c**) RMSF plot of dauricine. (**d**) Fractional interaction (occupancy) plot of SRC with dauricine. The Y-axis illustrates the total number of contact fractions for each residue at each simulation time. For instance, if a residue (indicated on the X-axis) maintains a single contact throughout the entire 100 ns simulation, its interaction score will be 1. Notably, LYS 298 has a score of approximately 1.6, indicating that it retains at least 1 contact point throughout the simulation. (**e**) Protein-ligand are represented along a time axis. (**f**) Protein-molecule interactions and hydrogen-bonding interactions are depicted by purple arrows.

bar plots normalized across trajectories (Figs. 9e and 10e), with ligands shaded in dark orange to highlight their spatial involvement.

The interaction diagram between protein and ligand (Figs. 9f and 10f) served as a vivid representation of the conformational stability and strong correlation within the protein-ligand complex. Notably, specific residues emerged as crucial contributors to these interactions. For dauricine and SLC6A3, HIS477, ARG85, ASP476,

GLY481, THR316, and ASP385 were identified as pivotal in the interaction, while for dauricine and SRC, ASP407, LYS298, HIS387, ARG391, and LEU410 played dominant roles. These findings significantly enhance our understanding of the molecular intricacies underpinning the potential therapeutic impact of dauricine on PD, offering valuable insights into the specific interactions governing its efficacy.

Discussion

In recent years, the exploration and application of traditional Chinese medicine compound preparations in neurodegenerative diseases have garnered extensive attention[46,47]. Network pharmacology provides a crucial framework for deciphering the intricate mechanisms underlying interactions among individual compounds within a formulation and their respective targets[48]. The field of Parkinson's drug discovery faces formidable challenges, encompassing the high costs associated with studies and a dearth of robust ADME profiles for novel drugs[49]. The complexity of PD pathophysiology, influenced by numerous factors, imposes limitations on conventional approaches such as dopamine replacement therapy and thalamic deep brain stimulation[5]. Chinese herbal medicine emerges as a promising repository of supplements for PD, leveraging a multi-target strategy. Notably, PCG have been a stalwart presence in PD treatment for decades, lauded for their minimal toxicity. Multiple clinical randomized controlled trials (RCTs) underscore the efficacy of PCG in complementing existing anti-Parkinson's drugs, pharmacological therapies, and functional surgeries[10–12]. However, the bioactive compounds within PCG and the mechanisms underpinning its anti-Parkinson's therapeutic effects remain elusive. To address this gap, we employed network pharmacology strategies, molecular docking, and simulations to delineate the potential action targets and mechanisms of PCG in PD.

In our investigation, we meticulously screened 96 active compounds associated with PCG from the TCMIP and HERB databases. Simultaneously, we curated a dataset comprising 477 PD targets, drawing from dopaminergic neuron bulkRNA-seq and snRNA-seq datasets, GeneCards, DisGeNET, and the TTD database. The culmination of this effort yielded a comprehensive identification of 96 anti-PD targets linked to PCG.

In our quest to unravel the intricate regulatory effects and specific mechanisms orchestrated by these anti-PD targets, we conducted a detailed functional enrichment analysis of pathways and functions associated with the identified targets. This analysis revealed a predominant enrichment of therapeutic targets within synaptic signal transduction pathways and G protein-coupled receptor (GPCR) signaling pathways. The current body of evidence substantiates the pivotal role of synaptic dysfunction in the evolution of PD. This is underscored by various phenomena, including dysfunctional synaptic vesicle endocytosis, contributing to the selective vulnerability of midbrain dopaminergic neurons[50]. Moreover, insights gleaned from imaging studies[51], postmortem brain immunohistochemical staining[52], and mechanistic studies in animal models[53] collectively suggest that synaptic damage and dysfunction precede neuronal loss by years, presenting themselves as viable therapeutic targets. A noteworthy discovery from a recent study on synaptic function in postmortem brain tissue from PD patients revealed enlarged surviving presynaptic terminals, indicative of a compensatory increase in mitochondrial numbers. This compensation mechanism is further underscored by a significant increase in total mitochondrial volume and the expression of mitochondrial complex I and IV subunits in PD, aiming to offset the loss of adjacent axonal terminals and maintain synaptic transmission[54].Given the acknowledged synaptic dysfunction and compensatory responses in PD, various clinical studies have been directed towards enhancing the synaptic function of dopamine neurons. Trophic factors, such as glial cell-derived trophic factor (GDNF), administered bilaterally intravesicular, have demonstrated efficacy in shortening the time to OFF in patients after 40 weeks[55]. The identified drug targets of PCG hold promise in effectively alleviating synaptic dysfunction and enhancing synaptic transmission signaling pathways.

Moreover, recent investigations have uncovered significant alterations in the GPCR signaling pathway among PD patients. Notably, dopamine receptors, a subset of GPCRs, play a crucial role in this pathway. These receptors bind to extracellular ligands, initiating a series of intracellular signaling cascades, primarily through their interaction with heterotrimeric G proteins[56]. Beyond dopamine receptors, numerous other GPCRs contribute to both the normal functioning and PD-related dysfunction of the striatum and basal ganglia, influencing neuronal circuits and intracellular signaling pathways[56]. Many GPCRs are actively under exploration as potential therapeutic targets for PD[57,58]. For instance, recent findings highlight the therapeutic efficacy of A2A-R antagonists targeting GPCRs, which have been successfully integrated into clinical strategies[59]. The spectrum of drug targets associated with PCG extensively encompasses dopamine receptors and other pathways mediated by GPCRs. While PCG may not singularly achieve a permanent alleviation of movement disorders in all patients solely through its impact on the G protein-coupled receptor signaling pathway, its combined therapy with other targets or medications holds the potential to offer broader and more effective coverage[56].

To further explore the 96 identified drug targets, we constructed a PPI network and identified 10 hub targets using a degree algorithm. Surprisingly, among these hub drug targets, we observed the inclusion of DRD2 and MAOB. Currently, drugs targeting MAO-B and DRD2 have achieved widespread use in the clinical management of PD patients. Dopamine receptor agonists such as ropinirole, pramipexole, and cabergoline effectively stimulate DRD2, alleviating motor symptoms in PD[60]. Moreover, MAO-B inhibitors like rasagiline, safinamide, and selegiline impact both motor and non-motor symptoms in PD patients[61]. Beyond these two targets, we maintain a strong belief in the pivotal roles played by the remaining eight drug targets in PCG's efficacy in alleviating clinical symptoms of PD. To validate our computational analysis, we conducted a meticulous comparison and analysis of the roles of these 10 hub drug targets in the onset and progression of PD, based on prior literature, as outlined in Table 2.

Additionally, we conducted co-expression and functional enrichment analyses on these 10 drug target genes. Intriguingly, these hub drug targets were found to be intricately linked to the ErbB signaling pathway. It is now well-established that ErbB signaling exerts control over the development and survival of dopaminergic neurons. Essential regulators within this pathway, such as epidermal growth factor (EGF) and neuregulin, along

Gene	Abstract	Citation
AKT1	Dysregulation of the Akt1-CREB pathway was observed in postmortem brain samples from individuals with PD. Activation of the Akt1-CREB pathway has the potential to prevent neurodegeneration in PD, as Akt1 can inhibit programmed cell death in dopaminergic neurons through a transcriptional mechanism.	Kim[62]
TNF	The level of TNF-α increased in the post mortem examination of the brain and cerebrospinal fluid of the patients with PD. TNFα binds to the TNFR1 receptor which leads to downstream activation of caspase 8 and caspase 3. Hence TNFR1 can lead to apoptosis of the dopaminergic neuron.	Amin[63]
SLC6A3	SLC6A3 encodes the dopamine transporter(DAT). DAT mainly presents on the neuron terminals in SN, and is necessary for dopaminergic neurotransmission to control its intensity and duration	Sossi[64]
MAOA	Monoamine oxidase (MAO) is one of the primary enzymes regulating metabolism of neurotransmitters such as dopamine. MAO-A is mainly responsible for regulating the phasic and tonic DA levels in the striatum by mediating DA degradation.	Cho[65]
IL1B	Increased IL-1β was revealed in both peripheral blood and CSF among patients with PD. Proinflammatory factors IL-1β can induce oxidative stress, neuronal death and in particular the loss of dopaminergic neurons in PD.	Qu[66]
IL6	Increased peripheral blood and CSF level of IL-6 was found in PD patients. The increased IL-6 level in the SN region and plasma are related to PD progression. Chronic exposure to IL-6 during neuronal development can lead to cell damage and death in a subpopulation of developing granule neurons.	Qu[66]
APP	β-amyloid precursor protein (APP) is a membrane-bound protein. The APP intracellular domain promotes LRRK2 expression and activates LRRK2-mediated neurotoxicity via FOXO3a.	Zhang[67]
MAOB	MAOB expression is significantly increased in the reactive astrocytes of the substantia nigra pars compacta (SNpc) in PD. Pharmacological blockade of MAOB inhibitors has been well documented to prevent MPTP-induced PD pathology and parkinsonian motor symptoms.	Moriguchi[68]
SRC	C-SRC is a ubiquitously expressed non-receptor tyrosine kinase. C-SRC promotes the release and uptake of α-syn and that c-src inhibition attenuates α-syn cell-to-cell transmission	Choi[69]
DRD2	DRD2 encodes the D2 subtype of the dopamine receptor. The mechanisms underlying DRD2-mediated immune response in PD may involve nucleotide-binding oligomerization domain-like receptor pyrin domain-containing 3 (NLRP3) inflammasome, renin-angiotensin system, and αB-crystallin.	Xia[70]

Table 2. Dysregulated expression and potential mechanisms of the 10 hub drug target genes in patients with PD.

with ErbB1-4 receptor tyrosine kinases, play pivotal roles in brain development and function. In the context of processes related to PD, postmortem analyses of PD brains have revealed reduced levels of EGF, a growth factor crucial for dopaminergic neurons, as well as diminished ErbB1 levels[71]. Furthermore, ErbB4 signaling in midbrain dopaminergic axonal projections has been implicated in regulating extracellular dopamine levels and influencing spatial/working memory behavior[72]. Consequently, it is conceivable that compounds within PCG may modulate the growth and development of dopaminergic neurons by regulating these 10 hub drug targets, subsequently impacting the spatial and working memory of individuals with PD.

To explore potential transcriptional level regulations in PD patients following changes in drug targets, we employed network tools to scrutinize the interactions between TFs, miRNAs, and genes. Our results indicate a robust regulatory relationship between TFs (FOXC1, GATA2, and TFAP2A) and miRNAs (hsa-mir-106a-5p, hsa-mir-34a-5p, and hsa-mir-203a-3p) with these 10 hub drug target genes. In a targeted methylation sequencing study on dopaminergic neurons, a reduction in protein expression of FOXC1, a gene associated with Wnt signaling and neurogenesis, was observed. This suggests the importance of epigenetic dysregulation in the Wnt signaling pathway in the pathogenesis of PD[73]. Concerning GATA-2, heightened expression in the substantia nigra of PD-susceptible patients, particularly within intron 1, was identified, regulating the expression of SNCA in DA neurons[74]. Additionally, studies revealed that ferroptosis stimulation in neurons induces the epigenetic induction of pro-survival genes through the transcription factor TFAP2, potentially contributing to the protection of neurons against ferroptosis[75]. Hence, it is plausible that TFAP2 may play a role in the anti-ferroptosis processes of dopaminergic neurons. An intriguing study examining non-coding RNA sequencing in Lund human midbrain neuronal cells overexpressing α-synuclein unveiled a substantial upregulation of hsa-miR-34a-5p, positioning it as a potential therapeutic target for PD[76]. Moreover, a separate investigation speculated through theoretical calculations that quercetin could exert a therapeutic effect on cognitive impairment and PD by influencing hsa-mir-203a-3p[77]. Through the analysis of hub transcription factors and miRNAs associated with hub drug targets, our findings suggest that PCG have the potential to alleviate both motor and non-motor symptoms in PD patients by acting on specific hub drug targets and inducing changes in transcription factors and miRNAs.

Using common drug target genes as a foundation, we constructed a network depicting the relationship between hub drug targets and diseases, providing insights into the correlations between these drug target genes and various medical conditions. These findings offer valuable guidance for potentially broadening the scope of PCG drug treatment indications. The established drug target gene-disease relationship network highlights associations with depression, a prevalent comorbid disease in PD. PCG exhibits the potential to act on IL1B, IL6, MAOB, and DRD2 drug targets, thereby alleviating depressive symptoms. Clinical trials of PCG drugs have consistently demonstrated the effectiveness of this approach in mitigating depressive symptoms in PD patients[11,12].Furthermore, our analysis indicates that the active compounds in PCG act on hub drug targets (IL1B, IL6, MAOB, APP), suggesting potential efficacy in ameliorating bipolar disorder. Robust evidence from numerous high-quality studies underscores a significantly heightened risk of PD development in patients with bipolar disorder[78–80]. Bipolar disorder emerges as a prodromal symptom in PD patients, and the shared pathophysiological mechanism, particularly the disruption of dopamine balance, links bipolar disorder and PD[81]. These insights lay a theoretical foundation for the therapeutic potential of PCG in addressing both depression and bipolar disorder, providing a promising avenue for future research and clinical exploration.

Additionally, an analysis of the transcriptional profiles of the 10 hub drug targets in the substantia nigra of PD patients and normal controls identified SLC6A3 and SRC as hub genes related to the pathogenesis of PD. These genes exhibited excellent disease diagnostic performance, with the constructed gene-based disease diagnosis model achieving AUCs of 0.954 in the training set and 0.910 and 0.838 in two independent validation sets, indicating robust generalization ability. Furthermore, molecular docking simulation analysis confirmed the stable binding affinity of bioactive compounds with these hub targets. Remarkably, dauricine demonstrated stable simultaneous binding to both SLC6A3 and SRC, with docking binding energies of -8.2 kcal/mol and − 10.2 kcal/mol, respectively. MD simulations over 100 ns further evaluated structural features and binding stability, revealing the persistent binding of dauricine to SLC6A3 and SRC. Thus, we posit that the active compound dauricine in PCG can effectively and stably act on SLC6A3 and SRC in the substantia nigra, two targets closely linked to the occurrence of PD.To explore the distribution of hub drug targets, such as SLC6A3 and SRC, in the substantia nigra of the midbrain in PD patients, we analyzed single-cell nuclei sequencing data sets. The findings confirmed that SLC6A3 and SRC are predominantly distributed in dopaminergic neurons within the midbrain.

To investigate the potential pathway modifications induced by dauricine acting on SLC6A3 and SRC proteins in dopaminergic neurons, we conducted single-gene GSEA. Intriguingly, the altered expression of these two genes was found to instigate changes in dopaminergic glucose metabolism-related pathways, specifically affecting glycolysis/gluconeogenesis and the pentose phosphate pathway. Current scientific investigations affirm glycolysis as a promising therapeutic target for PD[82]. Studies have consistently identified impairments in glycolysis, mitochondrial function, and lipid metabolism in both neural and non-neuronal cells of PD patients[83]. This impairment in energy supply processes, including glycolytic dysfunction, tricarboxylic acid (TCA) dysfunction, and oxidative phosphorylation, collectively diminish energy production, leading to neuronal dysfunction and degeneration—a crucial aspect of PD pathogenesis[84]. Moreover, multiple PET scan studies have reported impaired glucose uptake and glycolysis in the brains of PD patients, particularly evident in both cortical and substantia nigra regions[85,86]. This dysregulation in glycolysis has also been observed in genetic and toxin models of PD[87,88]. A recent breakthrough highlighted the enzyme PGK-1, a hub player in ATP production through glycolysis[88,89]. Its activation stimulates glycolysis, enhances ATP production, mitigates dopaminergic neuron loss, elevates dopamine levels, alleviates PD-related symptoms and complications, and decelerates disease progression[90]. The absence or low expression of PGK-1 emerges as a significant factor in PD etiology. Based on these findings, we posit that dauricine, the active compound in PCG, may act on SLC6A3 and SRC, thereby promoting glucose metabolism-related pathways in dopaminergic neurons and exerting a neuroprotective effect.

We acknowledge several limitations in our study that warrant consideration. The datasets analyzed from GEO, including bulk RNA-seq and single-cell sequencing data, may be subject to biases such as sample heterogeneity, small sample sizes, and differences in experimental protocols, which could introduce variability despite stringent quality control and batch correction. Additionally, the computational tools employed—network pharmacology, enrichment analysis, and molecular docking—have inherent constraints. Network pharmacology relies on the completeness of available databases, which may not capture all relevant biological interactions. Enrichment analysis is dependent on curated reference databases, potentially limiting the scope of pathway insights. Similarly, molecular docking and simulations, while informative, are based on static models and may not fully reflect the dynamic and complex nature of biological systems. These limitations underscore the importance of interpreting our findings within the context of these methodological constraints, while recognizing that the integrative approach used provides robust and meaningful insights into the therapeutic potential of Pingchan Granules in Parkinson's disease.

Our integrated approach, combining network pharmacology and bioinformatics analysis, elucidates the multi-target pharmacological mechanisms of PCG in Parkinson's disease and provides a strong scientific basis for its therapeutic potential. While our findings are supported by computational analyses, including gene expression profiling, machine learning, and molecular docking simulations, these methods are inherently predictive. Experimental validation through rigorous in vivo and in vitro studies is essential to confirm the functional relevance of the identified targets and pathways, as well as the therapeutic efficacy of PCG. Such studies are critical to bridge the gap between computational predictions and clinical applications.

Conclusion

In summary, this study employed network pharmacology and bioinformatics methodologies to comprehensively investigate the active compounds, potential targets, and mechanisms underlying the therapeutic effects of PCG in PD. It is noteworthy that our discoveries suggest that PCG, particularly through its hub compound dauricine, might modulate crucial targets within dopaminergic neurons (specifically, SLC6A3 and SRC), impacting glucose metabolism pathways. These effects contribute to a neuroprotective role, underscoring the significant therapeutic potential of PCG in PD treatment. Collectively, this research is poised to inform and advance the further development of PCG as a therapeutic intervention for PD, offering insights into its multi-compound, multi-pathway properties and mechanisms of action.

Data availability

All data generated or analysed during this study are included in this published article (and its Supplementary Information files).

Received: 14 December 2024; Accepted: 19 February 2025
Published online: 06 March 2025

References

1. Pagonabarraga, J., Kulisevsky, J., Strafella, A. P. & Krack, P. Apathy in Parkinson's disease: Clinical features, neural substrates, diagnosis, and treatment. *Lancet Neurol.* **14**, 518–531 (2015).
2. Onisiforou, A. & Spyrou, G. M. Immunomodulatory effects of microbiota-derived metabolites at the crossroad of neurodegenerative diseases and viral infection: Network-based bioinformatics insights. *Front. Immunol.* **13**, 843128 (2022).
3. Cocoros, N. M. et al. Long-term risk of Parkinson disease following influenza and other infections. *JAMA Neurol.* **78**, 1461–1470 (2021).
4. Onisiforou, A. & Spyrou, G. M. Systems bioinformatics reveals possible relationship between COVID-19 and the development of neurological diseases and neuropsychiatric disorders. *Viruses* **14**, 2270 (2022).
5. Armstrong, M. J. & Okun, M. S. Diagnosis and treatment of Parkinson disease: A review. *Jama* **323**, 548–560 (2020).
6. Schapira, A. H., Chaudhuri, K. R. & Jenner, P. Non-motor features of Parkinson disease. *Nat. Rev. Neurosci.* **18**, 435–450 (2017).
7. Christodoulou, C. C., Onisiforou, A., Zanos, P. & Papanicolaou, E. Z. Unraveling the transcriptomic signatures of Parkinson's disease and major depression using single-cell and bulk data. *Front. Aging Neurosci.* **15**, 1273855 (2023).
8. Ellis, T. D. et al. Identifying clinical measures that most accurately reflect the progression of disability in Parkinson disease. *Parkinsonism Relat. Disord.* **25**, 65–71 (2016).
9. Dorsey, E. R. et al. Global, regional, and National burden of Parkinson's disease, 1990–2016: A systematic analysis for the global burden of disease study 2016. *Lancet Neurol.* **17**, 939–953 (2018).
10. Ye, Q., Yuan, X. L., Yuan, C. X., Zhang, H. Z. & Yang, X. M. Zishenpingchan granules for the treatment of Parkinson's disease: A randomized, double-blind, placebo-controlled clinical trial. *Neural Regeneration Res.* **13**, 1269 (2018).
11. Gu, S. C. et al. Traditional Chinese medicine Pingchan granule for motor symptoms and functions in Parkinson's disease: A multicenter, randomized, double-blind, placebo-controlled study. *Phytomedicine* **108**, 154497 (2023).
12. Gu, S. C. et al. Pingchan granule for motor symptoms and Non-Motor symptoms of Parkinson's disease: A randomized, double-blind, placebo-controlled study. *Front. Pharmacol.* **13**, 739194 (2022).
13. Noor, F., Asif, M., Ashfaq, U. A. & Qasim, M. & Tahir Ul Qamar, M. Machine learning for synergistic network pharmacology: A comprehensive overview. *Brief. Bioinform.*, bbad120 (2023).
14. Noor, F. et al. Network Pharmacology approach for medicinal plants: Review and assessment. *Pharmaceuticals* **15**, 572 (2022).
15. Xu, H. Y. et al. Exploiture and application of an internet-based computation platform for integrative pharmacology of traditional Chinese medicine. *Zhongguo Zhong Yao Za Zhi = Zhongguo Zhongyao Zazhi = China J. Chin. Materia Med.* **42**, 3633–3638 (2017).
16. Fang, S. et al. HERB: A high-throughput experiment-and reference-guided database of traditional Chinese medicine. *Nucleic Acids Res.* **49**, D1197–D1206 (2021).
17. Kim, S. et al. PubChem in 2021: New data content and improved web interfaces. *Nucleic Acids Res.* **49**, D1388–D1395 (2021).
18. Daina, A., Michielin, O. & Zoete, V. SwissTargetPrediction: Updated data and new features for efficient prediction of protein targets of small molecules. *Nucleic Acids Res.* **47**, W357–W364 (2019).
19. UniProt. The universal protein knowledgebase in 2021. *Nucleic Acids Res.* **49**, D480–D489 (2021).
20. Barrett, T. et al. NCBI GEO: Archive for functional genomics data sets—update. *Nucleic Acids Res.* **41**, D991–D995 (2012).
21. Tiklová, K. et al. Disease duration influences gene expression in neuromelanin-positive cells from Parkinson's disease patients. *Front. Mol. Neurosci.* **14**, 763777 (2021).
22. Zaccaria, A. et al. Multiomic analyses of dopaminergic neurons isolated from human substantia Nigra in Parkinson's disease: A descriptive and exploratory study. *Cell. Mol. Neurobiol.*, 1–14 (2022).
23. Zhang, Y., James, M., Middleton, F. A. & Davis, R. L. Transcriptional analysis of multiple brain regions in Parkinson's disease supports the involvement of specific protein processing, energy metabolism, and signaling pathways, and suggests novel disease mechanisms. *Am. J. Med. Genet. Part. B: Neuropsychiatric Genet.* **137**, 5–16 (2005).
24. Lesnick, T. G. et al. A genomic pathway approach to a complex disease: Axon guidance and Parkinson disease. *PLoS Genet.* **3**, e98 (2007).
25. Kamath, T. et al. Single-cell genomic profiling of human dopamine neurons identifies a population that selectively degenerates in Parkinson's disease. *Nat. Neurosci.* **25**, 588–595 (2022).
26. Smajić, S. et al. Single-cell sequencing of human midbrain reveals glial activation and a Parkinson-specific neuronal state. *Brain* **145**, 964–978 (2022).
27. Safran, M. et al. GeneCards Version 3: The human gene integrator. *Database* (2010). (2010).
28. Piñero, J. et al. DisGeNET: A comprehensive platform integrating information on human disease-associated genes and variants. *Nucleic Acids Res.*, gkw943 (2016).
29. Wang, Y. et al. Therapeutic target database 2020: Enriched resource for facilitating research and early development of targeted therapeutics. *Nucleic Acids Res.* **48**, D1031–D1041 (2020).
30. Kuleshov, M. V. et al. Enrichr: A comprehensive gene set enrichment analysis web server 2016 update. *Nucleic Acids Res.* **44**, W90–W97 (2016).
31. Kanehisa, M., Furumichi, M., Sato, Y., Matsuura, Y. & Ishiguro-Watanabe, M. KEGG: Biological systems database as a model of the real world. *Nucleic Acids Res.* **53**, D672–D677 (2025).
32. Kanehisa, M. Toward understanding the origin and evolution of cellular organisms. *Protein Sci.* **28**, 1947–1951 (2019).
33. Kanehisa, M. & Goto, S. KEGG: Kyoto encyclopedia of genes and genomes. *Nucleic Acids Res.* **28**, 27–30 (2000).
34. Szklarczyk, D. et al. The STRING database in 2023: Protein–protein association networks and functional enrichment analyses for any sequenced genome of interest. *Nucleic Acids Res.* **51**, D638–D646 (2023).
35. Shannon, P. et al. Cytoscape: A software environment for integrated models of biomolecular interaction networks. *Genome Res.* **13**, 2498–2504 (2003).
36. Franz, M. et al. GeneMANIA update 2018. *Nucleic Acids Res.* **46**, W60–W64 (2018).
37. Zhou, G. et al. NetworkAnalyst 3.0: A visual analytics platform for comprehensive gene expression profiling and meta-analysis. *Nucleic Acids Res.* **47**, W234–W241 (2019).
38. Castro-Mondragon, J. A. et al. JASPAR 2022: The 9th release of the open-access database of transcription factor binding profiles. *Nucleic Acids Res.* **50**, D165–D173 (2022).
39. Huang, H. Y. et al. MiRTarBase update 2022: An informative resource for experimentally validated miRNA–target interactions. *Nucleic Acids Res.* **50**, D222–D230 (2022).
40. Biau, G. & Scornet, E. A random forest guided tour. *Test* **25**, 197–227 (2016).
41. Robin, X. et al. pROC: an open-source package for R and S + to analyze and compare ROC curves. *BMC Bioinform.* **12**, 1–8 (2011).
42. Morris, G. M., Huey, R. & Olson, A. J. Using Autodock for ligand-receptor docking. *Curr. Protocols Bioinf.* **24**, 81411–181440 (2008).
43. Seeliger, D. & de Groot, B. L. Ligand Docking and binding site analysis with PyMOL and Autodock/Vina. *J. Comput. Aided Mol. Des.* **24**, 417–422 (2010).
44. Zhu, Z. et al. Integration of summary data from GWAS and eQTL studies predicts complex trait gene targets. *Nat. Genet.* **48**, 481–487 (2016).
45. Pantsar, T. & Poso, A. Binding affinity via docking: Fact and fiction. *Molecules* **23**, 1899 (2018).
46. Moreira, J. et al. The neuroprotective effect of traditional Chinese medicinal plants—A critical review. *Acta Pharm. Sinica B* (2023).
47. Wang, Z. Y. et al. Traditional Chinese medicine compounds regulate autophagy for treating neurodegenerative disease: A mechanism review. *Biomed. Pharmacother.* **133**, 110968 (2021).

48. Shao, L. & Zhang, B. Traditional Chinese medicine network pharmacology: Theory, methodology and application. *Chin. J. Nat. Med.* **11**, 110–120 (2013).
49. Honorio, M., Moda, K. L., Andricopulo, D. & T. & Pharmacokinetic properties and in Silico ADME modeling in drug discovery. *Med. Chem.* **9**, 163–176 (2013).
50. Nguyen, M., Wong, Y. C., Ysselstein, D., Severino, A. & Krainc, D. Synaptic, mitochondrial, and lysosomal dysfunction in Parkinson's disease. *Trends Neurosci.* **42**, 140–149 (2019).
51. Nandhagopal, R. et al. Longitudinal evolution of compensatory changes in striatal dopamine processing in Parkinson's disease. *Brain* **134**, 3290–3298 (2011).
52. Kordower, J. H. et al. Disease duration and the integrity of the nigrostriatal system in Parkinson's disease. *Brain* **136**, 2419–2431 (2013).
53. Lundblad, M., Decressac, M., Mattsson, B. & Björklund, A. Impaired neurotransmission caused by overexpression of α-synuclein in nigral dopamine neurons. *Proc. Natl. Acad. Sci.* **109**, 3213–3219 (2012).
54. Reeve, A. K. et al. Mitochondrial dysfunction within the synapses of substantia Nigra neurons in Parkinson's disease. *Npj Parkinson's Disease*. **4**, 9 (2018).
55. Marks, W. J. et al. Gene delivery of AAV2-neurturin for Parkinson's disease: A double-blind, randomised, controlled trial. *Lancet Neurol.* **9**, 1164–1172 (2010).
56. Jones-Tabah, J. Targeting G protein-coupled receptors in the treatment of Parkinson's disease. *J. Mol. Biol.*, 167927 (2022).
57. Tison, F. et al. A phase 2A trial of the novel mGluR5-negative allosteric modulator dipraglurant for levodopa-induced dyskinesia in Parkinson's disease. *Mov. Disord.* **31**, 1373–1380 (2016).
58. Grégoire, L. et al. The acute antiparkinsonian and antidyskinetic effect of AFQ056, a novel metabotropic glutamate receptor type 5 antagonist, in l-Dopa-treated parkinsonian monkeys. *Parkinsonism Relat. Disord.* **17**, 270–276 (2011).
59. Chen, J. F. & Cunha, R. A. The belated US FDA approval of the adenosine A 2A receptor antagonist Istradefylline for treatment of Parkinson's disease. *Purinergic Signal.* **16**, 167–174 (2020).
60. Agúndez, J. A., García-Martín, E., Alonso-Navarro, H. & Jiménez-Jiménez, F. J. Anti-Parkinson's disease drugs and Pharmacogenetic considerations. *Expert Opin. Drug Metab. Toxicol.* **9**, 859–874 (2013).
61. Tan, Y. Y., Jenner, P. & Chen, S. D. Monoamine oxidase-B inhibitors for the treatment of Parkinson's disease: Past, present, and future. *J. Parkinson's Disease* **12**, 477–493 (2022).
62. Kim, H. et al. Activation of the Akt1-CREB pathway promotes RNF146 expression to inhibit PARP1-mediated neuronal death. *Sci. Signal.* **13**, eaax7119 (2020).
63. Amin, R. et al. The role of tumour necrosis factor in neuroinflammation associated with Parkinson's disease and targeted therapies. *Neurochem. Int.* **158**, 105376 (2022).
64. Sossi, V. et al. Dopamine transporter relation to dopamine turnover in Parkinson's disease: A positron emission tomography study. *Annals Neurology: Official J. Am. Neurol. Association Child. Neurol. Soc.* **62**, 468–474 (2007).
65. Cho, H. U. et al. Redefining differential roles of MAO-A in dopamine degradation and MAO-B in tonic GABA synthesis. *Exp. Mol. Med.* **53**, 1148–1158 (2021).
66. Qu, Y. et al. A systematic review and meta-analysis of inflammatory biomarkers in Parkinson's disease. *Npj Parkinson's Disease*. **9**, 18 (2023).
67. Zhang, Z. W. et al. The APP intracellular domain promotes LRRK2 expression to enable feed-forward neurodegenerative mechanisms in Parkinson's disease. *Sci. Signal.* **15**, eabk3411 (2022).
68. Nam, M. H., Sa, M., Ju, Y. H., Park, M. G. & Lee, C. J. Revisiting the role of astrocytic MAOB in Parkinson's disease. *Int. J. Mol. Sci.* **23**, 4453 (2022).
69. Choi, Y. R. et al. The dual role of c-src in cell-to-cell transmission of α-synuclein. *EMBO Rep.* **21**, e48950 (2020).
70. Xia, Q. P., Cheng, Z. Y. & He, L. The modulatory role of dopamine receptors in brain neuroinflammation. *Int. Immunopharmacol.* **76**, 105908 (2019).
71. Iwakura, Y. et al. Influences of dopaminergic lesion on epidermal growth factor-ErbB signals in Parkinson's disease and its model: Neurotrophic implication in nigrostriatal neurons. *J. Neurochem.* **93**, 974–983 (2005).
72. Skirzewski, M. et al. ErbB4 signaling in dopaminergic axonal projections increases extracellular dopamine levels and regulates spatial/working memory behaviors. *Mol. Psychiatry* **23**, 2227–2237 (2018).
73. Zhang, L. et al. Targeted methylation sequencing reveals dysregulated Wnt signaling in Parkinson disease. *J. Genet. Genom.* **43**, 587–592 (2016).
74. Scherzer, C. R. et al. GATA transcription factors directly regulate the Parkinson's disease-linked gene α-synuclein. *Proceedings of the National Academy of Sciences* **105**, 10907–10912 (2008).
75. Rroji, O., Kumar, A., Karuppagounder, S. S. & Ratan, R. R. Epigenetic regulators of neuronal ferroptosis identify novel therapeutics for neurological diseases: HDACs, transglutaminases, and HIF Prolyl hydroxylases. *Neurobiol. Dis.* **147**, 105145 (2021).
76. Findeiss, E. et al. Comprehensive miRNome-wide profiling in a neuronal cell model of synucleinopathy implies involvement of cell cycle genes. *Front. Cell. Dev. Biology*. **9**, 561086 (2021).
77. Duc Nguyen, H. Neurotherapeutic effects of Quercetin and its metabolite compounds on cognitive impairment and Parkinson's disease: An in Silico study. *Eur. J. Drug Metab. Pharmacokinet.* **48**, 151–169 (2023).
78. Huang, M. H. et al. Bipolar disorder and risk of Parkinson disease: A nationwide longitudinal study. *Neurology* **92**, e2735–e2742 (2019).
79. Faustino, P. R. et al. Risk of developing Parkinson disease in bipolar disorder: A systematic review and meta-analysis. *JAMA Neurol.* **77**, 192–198 (2020).
80. Onofrj, M. et al. Preexisting bipolar disorder influences the subsequent phenotype of Parkinson's disease. *Mov. Disord.* **36**, 2840–2852 (2021).
81. Dols, A. & Lemstra, A. W. Parkinsonism and bipolar disorder. *Bipolar Disord.* **22**, 413 (2020).
82. Foltynie, T. Glycolysis as a therapeutic target for Parkinson's disease. *Lancet Neurol.* **18**, 1072–1074 (2019).
83. Naeem, U. et al. Glycolysis: The next big breakthrough in Parkinson's disease. *Neurotox. Res.* **40**, 1707–1717 (2022).
84. Saxena, U. Vol. 16 351–354 (Taylor & Francis, (2012).
85. Firbank, M. J. et al. Cerebral glucose metabolism and cognition in newly diagnosed Parkinson's disease: ICICLE-PD study. *J. Neurol. Neurosurg. Psychiatry*. **88**, 310–316 (2017).
86. Ruppert, M. C. et al. Network degeneration in Parkinson's disease: Multimodal imaging of nigro-striato-cortical dysfunction. *Brain* **143**, 944–959 (2020).
87. Bell, S. M. et al. Peripheral Glycolysis in neurodegenerative diseases. *Int. J. Mol. Sci.* **21**, 8924 (2020).
88. Morales-Briceño, H. et al. Parkinsonism in PGK1 deficiency implicates the glycolytic pathway in nigrostriatal dysfunction. *Parkinsonism Relat. Disord.* **64**, 319–323 (2019).
89. Sakaue, S. et al. Early-onset parkinsonism in a pedigree with phosphoglycerate kinase deficiency and a heterozygous carrier: Do PGK-1 mutations contribute to vulnerability to parkinsonism? *Npj Parkinson's Disease*. **3**, 13 (2017).
90. Cai, R. et al. Enhancing Glycolysis attenuates Parkinson's disease progression in models and clinical databases. *J. Clin. Investig.* **129**, 4539–4549 (2019).

Acknowledgements
The authors express their gratitude to all study participants for their invaluable contribution to GEO resources by providing bulk RNA-seq and snRNA-seq data for analysis. Special thanks to TCMIP, PubChem, HERB, and the Swiss Target Prediction databases for providing a robust foundation in elucidating the active chemical components and targets of Pingchan Granules. We thank the Joint Fund for the National Natural Science Foundation of China, Joint Fund for Regional Innovation Development, (grant Number U23A20425) National Natural Science Foundation of China (grant number 82271268), National Key R&D Program (14th Five-Year Plan) (grant number SQ2022YFE020771), SQ2022YFE020771and Zhejiang Provincial Natural Science Foundation of China (grant number LY24H090003) supported this study.

Third party material
We have obtained formal permission from Kanehisa Laboratories to use KEGG pathway data and imagery under an Open Access license, adhering to their copyright and citation guidelines.

Author contributions
QX, YW collecteQX, YW collected, analyzed the data and wrote the manuscript. CW Visualization,, Validation, Data Management. JT and SJ conceptualized and oversaw the study and data analysis. JT and BZ provided funding supports. QiuHan Xu, YiLing Wang and Cheng Wang contributed equally to this article. All authors have read and approved the final manuscript.d, analyzed the data and wrote the manuscript. CW Visualization,, Validation, Data Management. JT and SJ conceptualized and oversaw the study and data analysis. JT and BZ provided funding supports. QiuHan Xu, YiLing Wang and Cheng Wang contributed equally to this article. All authors have read and approved the final manuscript.

Funding
This work was supported by grants from the National Natural Science Foundation of China, Joint Fund for Regional Innovation Development, (grant Number U23A20425) National Natural Science Foundation of China (grant number 82271268) ,National Key R&D Program (14th Five-Year Plan) (grant number SQ2022YFE020771), SQ2022YFE020771and Zhejiang Provincial Natural Science Foundation of China (grant number LY24H090003).

Declarations

Competing interests
The authors declare no competing interests.

Additional information
Supplementary Information The online version contains supplementary material available at https://doi.org/10.1038/s41598-025-91344-x.

Correspondence and requests for materials should be addressed to B.-R.Z. or J.T.